ABSTRACT

KANJ, HOUSSAM. Circuit-Level Modeling of Laser Diodes. (Under the direction of Dr. Michael B. Steer.)

In all semiconductor laser diodes the thermal, electrical, and optical characteristics are integrally related. In this work, a new approach to the modeling of laser diodes that integrates electrical, optical and thermal effects is presented. Also, it is demonstrated how physical device models based on complex differential equations can be easily implemented in the object oriented circuit simulator *f*REEDA™. Implementations of a Double-Heterojunction Laser Diode (DHLD) and a Vertical Cavity Surface Emitting Laser (VCSEL) diode are described. Simulations and results for both the DHLD and the VCSEL diodes are presented for DC, transient, and Harmonic-Balance analyses.

CIRCUIT-LEVEL MODELING OF LASER DIODES

by

HOUSSAM KANJ

A thesis submitted to the Graduate Faculty of
North Carolina State University
in partial fulfillment of the
requirements for the Degree of
Master of Science

Electrical Engineering

Raleigh

May 2003

APPROVED BY:

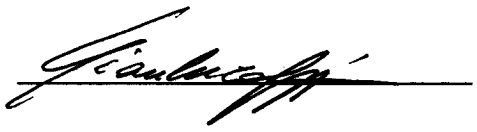

Chair of Advisory Committee

BIOGRAPHY

Houssam Kanj was born in Cairo, Egypt in 1977. He grew up in Beirut, Lebanon where he also received the B.S. in Computer and Communication Engineering in 1999 from The American University of Beirut, Lebanon. From July 1999 to December 2000 he worked as a system engineer with Tabbara Telecommunications, Lebanon. He joined North Carolina State University in Summer 2001 for the Master of Science program in Electrical Engineering. While working toward his M.S.E.E. degree he held a Research Assistantship with the Electronic Research Laboratory in the Department of Electrical and Computer Engineering. His research interests are in the fields of analog circuit design and computer-aided modeling of nonlinear circuits including electro-thermal and lasers.

ACKNOWLEDGEMENTS

I would like to express my appreciation to my advisor Dr. Michael Steer for guidance and support during my graduate studies. I would also like to thank Dr. Paul Franzon and Dr. Gianluca Lazzi for serving on my committee.

I would also like to thank Dr. Carlos Christofferson for his work on creating an excellent circuit simulator. Also, great thanks to Dr. Mark Neifeld and Mr. Ravi Pant at the University of Arizona for helping me understand the physics of laser diodes.

Finally, I would like to thank my family and friends for all the support and encouragement they gave me.

Contents

List of Figures

List of Tables

Chapter 1

Introduction

1.1 Motivation

Semiconductor laser diodes are being implemented in optoelectronic integrated circuits (OEIC's) for applications such as fiber optic communication and optical interconnections [1]. Motivated by the increasing interest in recent years to be able to simulate the electrical and optical properties of laser diodes, and the ability to perform both DC and transient simulations of these devices, different equivalent circuit models have been developed. In many cases these models were constructed as subcircuits in SPICE/HSPICE® from primitive elements such as nonlinear controlled sources, resistors and capacitors. While it is not very difficult to implement simple models in this approach, it becomes increasingly difficult and cumbersome to implement physically realistic and complicated ones since the primitive based models (*i.e.* using R, L, C, and controlled sources) are not able to model many physical effects [2].

Development of accurate models of such devices and components and the ability to easily implement them in circuit simulators in a compact and accurate way is greatly desirable. In this work, we demonstrate how physical device models based on complex differential equations can be easily implemented in the object-oriented circuit simulator *f*REEDA™ [3]. This is done with the capability of universal parameterized device modeling in conjunction with the local reference terminal concept coupled with *f*REEDA™'s ability to perform transient, DC and steady-state based analyses using

the same model.

*f*REEDA™ is a circuit simulator that provides a greatly simplified environment for model development of all kinds be it electrical, electromagnetic, thermal, or optical. In its object-oriented design, all kinds of elements can be considered as objects, and all these elements are connected to each other just like nodes and edges in a circuit graph. Hence the concept of OO (Object-oriented) programming maps directly onto circuit simulation. *f*REEDA™ also makes extensive use of support libraries that reduces further the amount of code needed. Specifically, the use of the ADOL-C [4] library avoids the need to perform derivative evaluations within the device model code and enables the same model code to be used with various types of analysis including transient, DC, and harmonic balance. This makes the process of writing models for *f*REEDA™ relatively straightforward. *f*REEDA™ also has the capability to support various type of analysis such as DC, transient, and harmonic balance for the same model (*i.e.* computer code). This in effect simplifies the process of model modification and maintenance.

1.2 Thesis Overview

Chapter 2 describes laser diode modeling and provides a brief history. It also gives a brief overview of *f*REEDA™, the circuit simulator for which the laser diodes models had been written. Features that simplify the model writing process are described.

Chapter 3 describes the implementation of the Double-Heterojunction Laser Diode (DHLD) in *f*REEDA™ and presents simulation results for different types of circuit analysis (*i.e. DC, Transient, and Harmonic Balance*). The results shows an excellent agreement with HSPICE® when it is possible using simplified models.

Chapter 4 describes in detail the implementation of the Vertical Cavity Surface Emitting Laser (VCSEL) diode in *f*REEDA™ and presents simulation results for different types of circuit analysis. The results shows an excellent agreement with the available measurement. Finally, the VCSEL nonlinearity is studied as a function of temperature and bias current.

Chapter 5 summarizes the work presented in this thesis. It outlines future research

plans involving simulations of packaged VCSEL diode arrays and optoelectronic integrated circuits with Electro-Opto-Thermal interaction and optical feedback.

1.3 Original Contributions

The DHLD model in *f*REEDA™ is unique in its implementation. The proper choice of state variables with the equation parameterization discussed in Sec. 3.4 resulted in excellent convergence properties with all analysis type be it DC, transient, or harmonic balance. Another original contribution was the implementation of the VCSEL model in *f*REEDA™. The device equations were normalized and variable transformations were used to improve the convergence properties of the model as shown in Sec. 4.4. The model was also modified to include the chirp equation and harmonic balance simulations were used to study the VCSEL nonlinear distortion and large signal chirp as a function of bias current and temperature.

Chapter 2

Literature Review

2.1 Introduction

Recent years have witnessed an increasing interest in optoelectronic integrated circuits and systems. As in the early days of electronic integrated circuits which led to the development of circuit simulators such as SPICE, there is an obvious need for efficient and accurate CAD tools for the simulation and design of OEIC's. While many tools exist which can be used for OEIC's simulations, they are mainly intended for electronics simulations. They also lack an easy-to-use and efficient modeling environment for optoelectronic components.

This chapter attempts to give a brief overview of laser diode modeling and how these models have been implemented in a general purpose circuit simulator. It also describes *f*REEDA™, the circuit simulator for which the laser diodes models had been written and highlights some of the features that enable the ease of model writing and model maintenance.

2.2 Laser Diode Modeling

The invention of the transistor has made semiconductor physics a hot topic in the 1950's and enabeled development of the semiconductor laser. Although light emission in semiconductors had already been known for half a century, it was not until 1962 [5]

that the first semiconductor laser was demonstrated, and not until 1970 [6] was the first continuous wave room temperature operation demonstrated. Soon after that, semiconductor laser diode found applications in fiber optic communication and it was clear that the simulation of such devices is necessary for the design of such systems.

Although several researchers have addressed the circuit level modeling of optoelectronic devices, not many commercial CAD companies have adapted such models into their software packages [7]. The implementation of such models is usually not straight forward and requires the ability to adapt the rate equations (in case of laser diodes) into their corresponding equivalent circuit elements. While this method does enable the user to implement a rate-equation based laser diode model for example, it has several drawbacks and it does not lend itself well for fast prototyping of new devices or new device features [2] and that is why analog behavioral modeling languages are of great importance for the implementation of such devices.

The key advantage of analog behavioral modeling tools is the simplicity of the design language used to model devices, circuits, and systems as a set of algebraic or differential equations which are subsequently solved in either DC, AC, transient analysis [2]. In addition, many researchers have addressed the computer aided design and analysis of optoelectronic circuits for microwave applications and that is why a circuit simulator that possess all of the above properties and have the ability to perform harmonic balance simulations and more is critical for the opto-electronic design community.

2.3 The fREEDA™ Circuit Simulator

2.3.1 Introduction

With the increasing speed and capacity of data transfer systems, there is a growing need for optical interconnection systems [8]. In designing optical interconnects, reliable and easy-to-use CAD tools are required that can handle both electrical and optical devices, and in many cases thermal and electromagnetic elements. That is, an easily extensible and modifiable computer aided engineering (CAE) tool is required

with a global modeling environment capabilities. In other words, the tool should be able to model devices, circuits and systems as a set of algebraic or differential equations which are subsequently solved in DC, AC, transient, or even Harmonic Balance analyses. A CAD tool that has most of the above desired features is *f*REEDA™. While this simulator was first designed as a microwave circuit simulator, it has clearly been shown that it is a global modelling environment. It is designed as an object-oriented (OO) circuit simulator which is one of the most significant developments relevant to computer aided engineering. While it is normal to think of OO-specific programming languages as being the main technology for implementing OO design, good OO practice can be implemented in more conventional programming languages such as C. However OO-specific languages foster code reuse and have constructs that facilitate object manipulation. The OO abstraction is well suited to modelling electronic systems, for example, circuit elements are already viewed as discrete objects and at the same time as an integral part of a (circuit) continuum. The OO view is a unifying concept that maps extremely well onto the way humans perceive the world around them.

The goal in defining the architecture of *f*REEDA™ was to obtain speed in development, to use off-the-shelf advanced numerical techniques, and to allow easy expansion and testing of new models and numerical methods. The circuit simulator implementing these ideas is *f*REEDA™. It is the first circuit simulator to use recent OO techniques. The design intent was to combine the advantages of previous OO circuit simulators with these new developments as well as expanding simulator capability. *f*REEDA™ uses libraries written in C++, C, and Fortran. These support libraries [9] are essential to the unique architecture of *f*REEDA™ and the most important of these libraries is related to derivative modeling and is described in the next section.

2.3.2 Automatic Differentiation

One of the most important features of *f*REEDA™ is the use of Automatic Differentiation. Most nonlinear computations require the evaluation of first and higher

derivatives of vector functions with m components in n real or complex variables. Often these functions are defined by sequential evaluation procedures involving many intermediate variables. By eliminating the intermediate variables symbolically, it is theoretically always possible to express the m dependent variables directly in terms of the n independent variables. Typically, however, the attempt results in unwieldy algebraic formulae, if it can be completed at all. Symbolic differentiation of the resulting formulae will usually exacerbate this problem of expression swell and often entails the repeated evaluation of common expressions. Most importantly, the manual development and coding of derivative expressions leads to code that is extremely difficult to check and debug.

An obvious way to avoid such redundant calculations is to apply an optimizing compiler to the source code that can be generated from the symbolic representation of the derivatives in question. Given a code for a function $F : \Re^n \longrightarrow \Re^m$, automatic differentiation (AD) uses the chain rule successively to compute the derivative matrix.

A versatile implementation of the AD technique is Adol-C [4], a software package written in C and C++. The numerical values of derivative vectors (required to fill a Jacobian for solving non-linear elements using Newtons method) are obtained free of truncation errors at a small multiple of the run time required to evaluate the original function with little additional memory required. It is important to note that AD is not numerical differentiation and the same accuracy achieved by evaluating analytically developed derivatives is obtained. In *f*REEDA™, the eval() method of the nonlinear element class is executed at initialization time and so the operations to calculate the currents and voltages of each element are recorded by Adol-C in a tape which is actually an internal buffer. After that, each time that the values or the derivatives of the nonlinear elements are required, an Adol-C function is called and the values are calculated using the tapes. This implementation is efficient because the taping process is done only once (this almost doubles the speed of the calculation compared to the case where the functions are taped each time they are needed). When the Jacobian is needed, the corresponding Adol-C function is called using the same tape. In the case of Harmonic Balance simulations, the program has been tested with large circuits with many tones, and the function or Jacobian evaluation times are always

very small compared with the time required to solve the matrix equation (typically some form of Newtons method) that uses the Jacobian. The conclusion is that there is little detriment to the performance of the program introduced by using automatic differentiation. However the advantage in terms of rapid model development is significant. The majority of the development time in implementing models in simulators, is in the manual development of the derivative equations. Unfortunately the determination of derivatives using numerical differences is not sufficiently accurate for any but the simplest circuits and in any event, is computationally intensive. With Adol-C full analytic accuracy is obtained and the implementation of new analysis is dramatically simplified. From experience the average time to develop and implement a transistor model is an order of magnitude less than deriving and coding the derivatives manually. Note that time differentiation, time delay and transformations are left outside the automatic differentiation block. The calculation speed achieved is approximately ten times faster than the speed achieved by including time differentiation, time delay and transformations inside the block.

Chapter 3

The Double Heterojunction Laser Diode Model

3.1 Introduction

This section considers a double-heterojunction laser diode (DHLD) device. The DHLD consists of a p-type GaAs active layer of thickness d sandwiched between n-type and p-type layers of higher bangap material as shown in Fig. 3.1. The circuit model for the DHLD is shown in Fig. 3.2. It is similar in many ways to the structure described in [10]. The laser diode model is based on the Tucker large-signal circuit model [11, 12]. It is derived from the physics of the heterojunction and explicitly takes into account the effect of carrier degeneracy, high level injection, and nonradiative recombination. The modulation response is determined through the rate equations of the device's electro-optical dynamics. The following sections describe the governing equations of the model and its implementation in *f*REEDA™.

3.2 Parameter Table

Table 3.1 lists the parameters used to model the DH Laser Diode in *f*REEDA™.

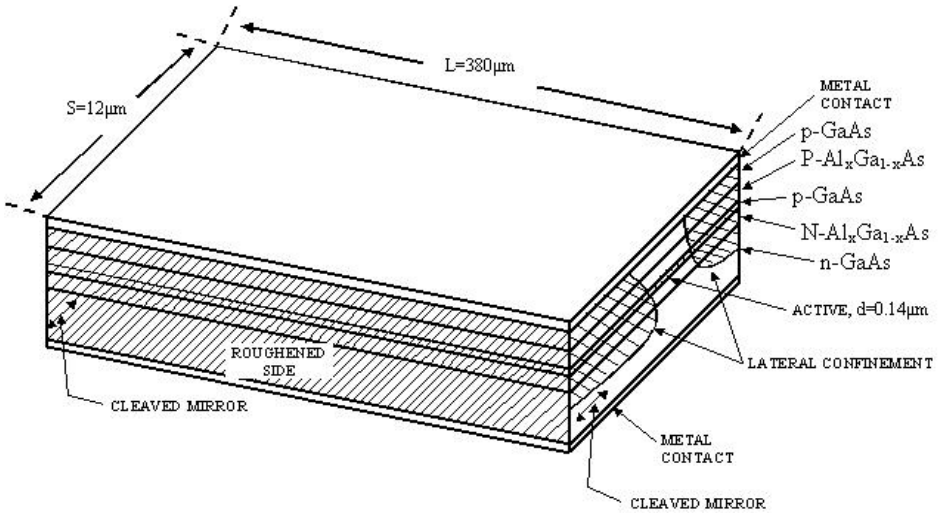

Figure 3.1: Double-heterostructure laser. The *p-GaAs* active layer is usually less than 0.5 μm thick. After [13, 14].

3.3 Analysis

Under the assumption that the thickness d of the active layer is small compared to the carrier diffusion length and that the variation of carrier densities with position in the active layer is small enough [11], the carrier densities can be represented by average values. Then the average total electron density N in the active layer is given by

$$N = N_0 + n \tag{3.1}$$

where N_0 is the equilibrium electron density and n is the excess electron density. Corresponding notation can be used for hole densities.

From the physics of the Heterostructure lasers [10, 11], and under the above assumptions, the total radiative spontaneous recombination rate R in the active layer is given by:

$$R = BNP \tag{3.2}$$

where B is a constant and P is the average total hole density in the active layer [11]. To obtain the diode current due to spontaneous radiative recombination, we define

Table 3.1: Parameters for the DH Laser Diode Model

Parameters	**Description**	**Values**	**Units**
R_s	series resistance	2	Ω
R_e	equivalent resistance due to carrier degeneracy	0.468	Ω
I_{01}	equivalent Diode1 leakage current	2.54e-25	A
I_{02}	equivalent Diode2 leakage current	18.13e-3	A
b	current controlled current source gain	6.92	A^{-1}
τ_{ns}	equivalent recombination Lifetime	2.25e-9	s
C_0	diode zero-bias charge capacitance	10e-12	F
V_D	junction built-in potential	1.65	V
D	constant relating the radiative recombination current per unit volume to the optical gain	1.79e-29	$V^{-1}A^{-1}m^6$
a	fraction of equivalent recombination lifetime over low-level injection spontaneous recombination lifetime	0.125	-
R_p	equivalent optical resistor	29.4	Ω
C_p	equivalent optical capacitor	0.102e-12	F
S_c	photon density normalization constant	1e21	m^{-3}
β	fraction of spontaneous emission coupled into the lasing mode	1e-3	-

the excess spontaneous radiative recombination rate r_e as:

$$r_e = n/\tau_s + B_1 n^2 \tag{3.3}$$

where τ_s is the low-level injection spontaneous recombination lifetime and B_1 is a constant defined in [11].

Also, a significant contribution to the diode current arises from nonradiative recombination rate r_n along the strip edges and at the heterointerfaces. Following the analysis in [10], it is assumed here that the nonradiative recombination rate is proportional to n, and is characterized by a lifetime τ_n. Then the total excess recombination rate r_t (including radiative and nonradiative components) is obtained by adding the nonradiative recombination rate $r_n = n/\tau_n$ to r_e:

$$r_t = (1/\tau_n + 1/\tau_s)n + B_1 n^2 \ . \tag{3.4}$$

Again, since the active layer is assumed to be thin, the diode recombination current is obtained by multiplying r_t by the active layer volume v_a and the electron charge

q. Adding to it the displacement-current term, we obtain the diode terminal current below threshold I:

$$I = qv_a \left(r_t + \frac{dn}{dt} \right) \ . \tag{3.5}$$

Note that Eqn. 3.5 does not include the effects of space-charge capacitance which will be considered in Sec. 3.3.2. Substituting Eqn. 3.4 in Eqn. 3.5 gives:

$$I = I_1 + bI_1^2 + \tau_{ns} \frac{dI_1}{dt} \tag{3.6}$$

where

$$I_1 = \frac{qv_a n}{\tau_{ns}} \tag{3.7}$$

$$b = \frac{B_1 \tau_{ns}^2}{qv_a} \tag{3.8}$$

and

$$\tau_{ns} = (\tau_s^{-1} + \tau_n^{-1})^{-1} \tag{3.9}$$

3.3.1 Current/Voltage characteristics

The diode junction voltage V_j can be expressed in terms of the electron density in the active layer as a three series-connected voltage drops V_1, V_2, and V_3. That is:

$$V_j = V_1 + V_2 + V_3 \tag{3.10}$$

and

$$V_1 = V_T \ln(1 + n/N_0) \tag{3.11}$$

$$V_2 = V_T \ln\{1 + n/(N_A + N_0)\} \tag{3.12}$$

$$V_3 = V_T(\alpha_1 + \alpha_3)n \tag{3.13}$$

where $V_T = kT/q$ is the thermal voltage, N_A is the acceptor impurity concentration, and α_1 and α_2 are constant defined in [11]. The first two of these elements represent a classical Shockley p-n junction diodes. With Eqn. 3.7 substituted, Eqns. 3.11 and 3.12 become:

$$I_1 = I_{01}\{\exp(V_1/V_T) - 1\} \tag{3.14}$$

and

$$I_1 = I_{02}\{\exp(V_2/V_T) - 1\} \tag{3.15}$$

where I_1 is the current through the two diodes and the two diode leakage currents are given by:

$$I_{01} = qv_aN_0/\tau_{ns} \tag{3.16}$$

and

$$I_{02} = qv_a(N_A + N_0)/\tau_{ns} \tag{3.17}$$

The third series-connected element is given by Eqn. 3.13. Substituting Eqn. 3.7 in Eqn. 3.13 gives

$$I_1 = V_3/R_e \tag{3.18}$$

where

$$R_e = (\alpha_1 + \alpha_3)N_0V_T/I_{01}\ . \tag{3.19}$$

3.3.2 Rate Equations

As mentioned earlier, the excess spontaneous recombination rate per unit volume r_t can be written as the sum of two components r_n and r_e:

$$r_t = r_n + r_e \tag{3.20}$$

Then, the total diode current due to spontaneous recombination is $I_t = qv_ar_t$, which can be written in the form:

$$I_t = I_1 + bI_1^2 \tag{3.21}$$

and the diode current due to radiative spontaneous recombination is $I_e = qv_ar_e$, which reduces to:

$$I_e = aI_1 + bI_1^2 \tag{3.22}$$

where

$$a = \tau_{ns}/\tau_s \tag{3.23}$$

The single mode rate equations for an injection laser [12] can be written in the form

$$qv_a\frac{dn}{dt} = I - I_t - qv_agS \tag{3.24}$$

$$qv_a \frac{dS}{dt} = qv_a gS - \frac{Sqv_a}{\tau_p} + \beta I_e \tag{3.25}$$

where I is the diode terminal current, g is the optical gain, S is the photon density in the active layer, τ_p is the photon lifetime, and β is the fraction of spontaneous emission coupled into the lasing mode. Eqn. 3.24 describes electron-injection and charge-storage effects in the active layer, and Eqn. 3.25 describes the corresponding injection and storage dynamics of photons. These equations form the basis of the equivalent large signal model. To account for the space-charge storage in the heterojunction layer, Eqn. 3.24 is generalized to include space-charge capacitance term. Note that this effect is taken into account by a capacitor C_s and is different from the charge-storage effect taken into account by the term $\tau_{ns} dI_1/dt$. Also, a normalized photon density S_n is introduced to obtain better numerical values. With the above modifications, and substituting Eqns. 3.21 and 3.22, the rate equations become:

$$I = I_1 + bI_1^2 + \tau_{ns} \frac{dI_1}{dt} + C_s \frac{dVj}{dt} + GS_n \tag{3.26}$$

$$GS_n + \beta(aI_1 + bI_1^2) = \frac{S_n}{R_p} + C_p \frac{dS_n}{dt} \tag{3.27}$$

where $C_s = C_0(1 - V_j/V_D)^{-1/2}$ is the space-charge capacitance, V_J is the heterojunction voltage, C_0 is the zero bias space-charge capacitance, V_D is the diode built-in potential, $C_P = qv_a S_c$, $G = gC_p$, $R_p = \tau_p/C_p$, and $S_n = S/S_c$, where S_c is the photon-density normalization constant.

3.3.3 Equivalent Large-signal Circuit Model

The large-signal circuit model of the injection laser follows from the rate equations, Eqns. 3.26 and 3.27, and from the current/voltage characteristics of the diode described in Sec. 3.3.1. The electrical equivalent model is shown to the left of the vertical broken line in Fig. 3.2. It is important to note that the resistance R_e in series with the two Shockley diodes arises from carrier degeneracy, and is not associated with the ohmic regions of the diode. Those regions are modelled by a series resistance R_s which includes contributions from lead resistance, bulk resistance in the high-bandgap materials, and the effective resistance of the near-ohmic p-P isotype heterojunction.

The resulting equivalent circuit model of the photon dynamics is shown to the right

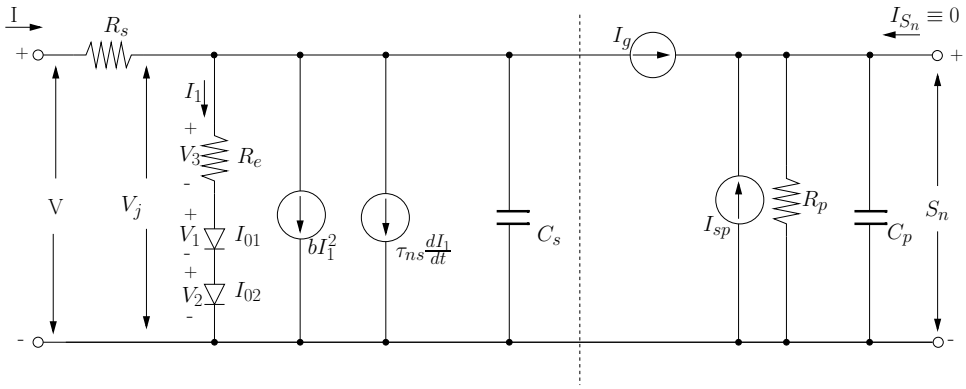

Figure 3.2: Large-signal two port circuit model of injection laser

of the vertical broken line in Fig. 3.2 and is derived from Eqn. 3.27. where

$$I_{sp} = \beta(aI_1^2 + bI_1^2) \tag{3.28}$$

and

$$I_g = GS_n \ . \tag{3.29}$$

3.3.4 Diode Parameters

The laser parameters used in the simulations are the same as the ones used in [11, 12], and are similar to the parameters used in [10]. The excess electron density in the active layer is assumed to be $n_s = 1.5 \times 10^{18}$ cm^{-3}, and the factor qv_a is taken as 1.02×10^{-25} mA cm^3 s. Thus the threshold current I_t is approximately 100 mA. The active layer doping density is taken as $N_A = 4 \times 10^{17}$ cm^{-3}, and the photon lifetime is $\tau_p = 3.0$ ps.

It is also assumed that the optical gain function G has a square-law dependence on the radiative recombination current per unit volume J_{nom} as described in [13]

$$G = D(J_{nom} - 2 \times 10^{13})^2 \tag{3.30}$$

where D is a constant and $J_{nom} = I_e/v_a$ A/m^3.A numerical value of D can be obtained by first determining S_{n0}, the steady-state normalized photon density, and then setting

it to infinity at saturation, that is when $n = n_s$. The steady-state photon density is obtained by subsrituting $dS_n/dt = 0$ in Eqn. 3.27

$$S_{n0} = \frac{\beta(aI_{10} + bI_{10}^2)}{1/R_p - G} \tag{3.31}$$

where I_{10} is the steady-state value of I_1. As we can see, S_{n0} goes to infinity when $G = 1/R_p$ which, when substituted in Eqn. 3.30, yields

$$D = R_p^{-1}(J_{noms} - 2 \times 10^{13})^{-2} \tag{3.32}$$

where J_{noms} is the value of J_{nom} at saturation, and is given by

$$J_{noms} = \frac{qn_s}{\tau_{ns}}(a + b\frac{qv_a n_s}{\tau_{ns}}) \tag{3.33}$$

with the known diode parameters substituted in Eqns. 3.33 and 3.30, we obtain $J_{noms} = 6.359 \times 10^{13}$ and $D = 1.79 \times 10^{-29}$ V^{-1} A^{-1} m^6. Numerical values of other parameters of the circuit model are listed in Table 3.1.

3.4 Implementation in fREEDA™

The key to the implementation of the model is to consider the voltage on one of the diodes in Fig. 3.2 as the first state variable, V_1 for example, and the normalized photon density S_n as the second state variable, and then write the model equations as a function of these two state variables and there derivatives, *i.e.* dV_1/dt and dS_n/dt .

The relation between the drive input voltage V and current I is given by:

$$V = IR_s + V_j \tag{3.34}$$

where I can be expressed as:

$$I = I_1 + bI_1^2 + \tau_{ns}\frac{dI_1}{dt} + C_s\frac{dV_j}{dt} + I_g \tag{3.35}$$

To write Eqns. 3.34 and 3.35 in terms of the state variables and there derivatives, we need to find I_1, dI_1/dt, V_j, and dV_j/dt in terms of these state variables. From Eqn. 3.14, we know that $I_1 = I_{01}\{\exp(V_1/V_T) - 1\}$, then

$$\frac{dI_1}{dt} = \frac{I_{01}}{V_T}\exp(V_1/V_T)\frac{dV_1}{dt} \tag{3.36}$$

and V_j can be expressed as:

$$V_j = V_1 + V_2 + V_3 \tag{3.37}$$

where

$$V_2 = V_T ln(I_1/I_{02} + 1) \tag{3.38}$$

and

$$V_3 = I_1 R_e \cdot \tag{3.39}$$

We still have to write dV_j/dt as a function of the state variables and their derivatives:

$$\frac{dV_j}{dt} = \frac{dV_1}{dt} + \frac{dV_2}{dt} + \frac{dV_3}{dt} \tag{3.40}$$

where from Eqn. 3.38, we have

$$\frac{dV_2}{dt} = \frac{I_{01}}{I_{02}} \exp\{\frac{(V_1 - V_2)}{V_T}\} \frac{dV_1}{dt} \tag{3.41}$$

and from Eqn. 3.39, we have

$$\frac{dV_3}{dt} = R_e \frac{dI_1}{dt} \ . \tag{3.42}$$

Finally, we have to find I_g as a function of the state variables. We know that $I_g = GS_n = D(J_{nom} - 2 \times 10^{13})^2 S_n$, and that $J_{nom} = I_e/v_a = (aI_1 + bI_1^2)/v_a$, then

$$I_g = D(\frac{aI_1 + bI_1^2}{v_a} - 2 \times 10^{13})^2 S_n \ . \tag{3.43}$$

Now that we have expressed the current I and voltage V at the electrical port of the diode as a function of the state variables, we have to express the current and voltage at the optical port of the diode as a function of those variables. The voltage at the optical port is chosen to be S_n, however, the current I_{sn} has no meaning and it is forced to be zero ($I_{sn} \equiv 0$) by connecting an open circuit to the optical port. The model, however, will not function properly unless the Eqn. 3.27 is satisfied. This is done by using the fact that $I_{sn} \equiv 0$ and by rewriting Eqn. 3.27 in the form[1]

$$I_{sn} = GS_n + \beta(aI_1 + bI_1^2) - \frac{S_n}{R_p} - C_p \frac{dS_n}{dt} \tag{3.44}$$

[1]Another way to satisfy Eqn. 3.27 is to connect a 1 Ω resistor at the optical port and make use of the fact that $I_{sn} - S_n \equiv 0$, where $I_{sn} = R_p GS_n + R_p \beta(aI_1 + bI_1^2) - R_p C_p \frac{dS_n}{dt}$. This implementation actually will not result in a singular matrix in Harmonic-balance simulations and alleviate the need to use a large resistance instead of the open circuit in that case.

As we can see, the implementation is quite simple and straightforward. This is mainly due to the use of OO-design in *f*REEDA™, and to automatic differentiation which replaces the need to code the partial derivatives.

One last thing we did not talk about above is parameterization or variable transformations. They both refer to an algebraic transformation of the device equations that leads to a better convergence properties, and enables universal device modeling. The parameterization employed here is the one suggested in [15] and that converts the strong nonlinear current-voltage relationship of the diode to two smoother functions of current and voltage as functions of the state-variable x. Specifically, V_1 is not taken as the state variable in the actual coding, and Eqn. 3.14 is parameterized as follows

$$I_1 = \begin{cases} I_{01}\{\exp(\alpha x) - 1\} & \text{if } x \leq V_{pr} \\ I_{01}\exp(\alpha V_{pr})\{1 + \alpha(x - V_{pr})\} - I_{01} & \text{if } x > V_{pr} \end{cases} \tag{3.45}$$

$$V_1 = \begin{cases} x & \text{if } x \leq V_{pr} \\ V_{pr} + \frac{1}{\alpha}\ln\{1 + \alpha(x - V_{pr})\} & \text{if } x > V_{pr} \end{cases} \tag{3.46}$$

where $\alpha = 1/V_T$ and V_{pr} plays the role of a free parameter chosen appropriately to optimize the performance of the HB algorithm specifically. Experience shows [15] that $V_{pr} = \ln(1/\alpha I_s)/\alpha$ results in excellent behavior of the model in most practical situations. As shown in Fig. 3.3, 3.4, and 3.5, the strong nonlinearity between i & v is converted to moderate nonlinearities between i & x and v & x, and the problem becomes well behaved. Please refer to [9] and [16] for more information on universal device modeling, and how the same piece of code is used in *f*REEDA™ with different simulation algorithms, *i.e.* HB, Transient, DC analysis, etc.

3.5 Simulations and Results

The following sections present the simulation results of the DHLD model implemented in *f*REEDA™. Sec. 3.5.1 presents the results of the transient analysis. The diode is driven by an input current pulse of finite rise and fall time. Graphs of the input terminal voltage and of the normalized photon density are shown for different values of β and compared with HSPICE®.

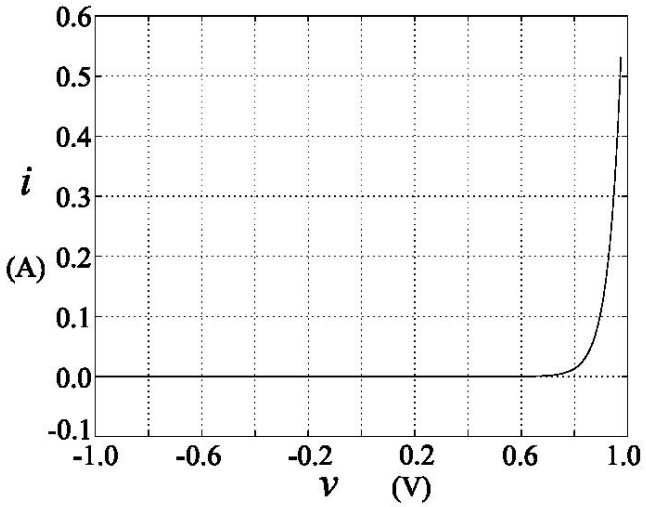

Figure 3.3: Relation between v and i in a diode.

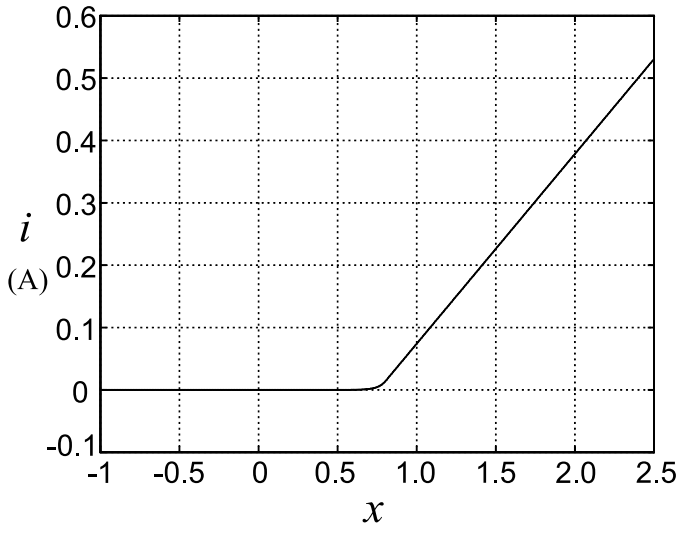

Figure 3.4: Relation between x and i in a diode.

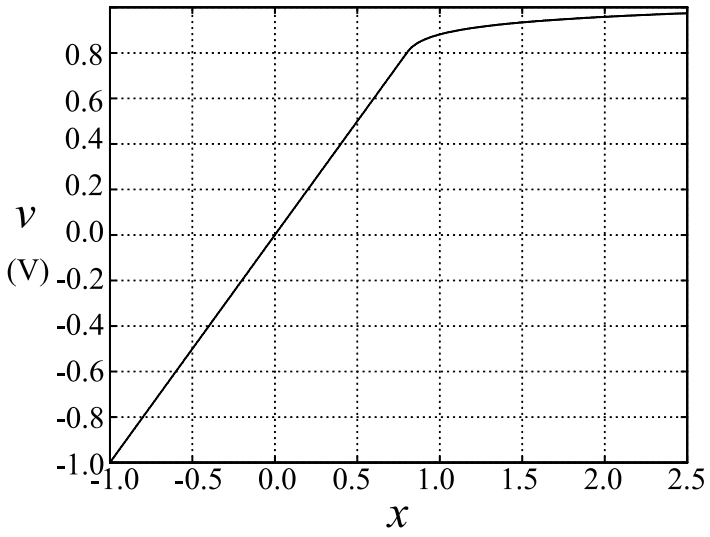

Figure 3.5: Relation between x and v in a diode.

In Sec. 3.5.2, a Harmonic Balance analysis is performed on the implemented DHLD model. First, the model is driven by a DC bias source and single tone sine wave. Plots of the input terminal voltage and of the normalized photon density are shown and compared with *f*REEDA™ 's transient analysis and HSPICE®. Second, the model is driven by a DC bias source and two tone input sine waves. Plots of the optical output power spectrum is presented. Also, the power ratio of the second harmonic to the fundamental P_{2f}/P_f and of the intermodulation distortion to the fundamental P_{IM3}/P_f as a function of bias current are shown.

The source code that implements the model, which consists of a C++ source file and a header file, can be found in Appendix A. The *f*REEDA™ netlists which was used to generate the plots in the following sections can be found in Appendix C.1.

3.5.1 Transient Analysis

In the analysis and design of laser diode transmitter, it is very important to determine laser turn-on delay and other switching and modulation characteristics especially for high-speed application where the switching waveform is affect by the finite bandwidth of the drive circuits [11]. This is why transient simulation is very important in the

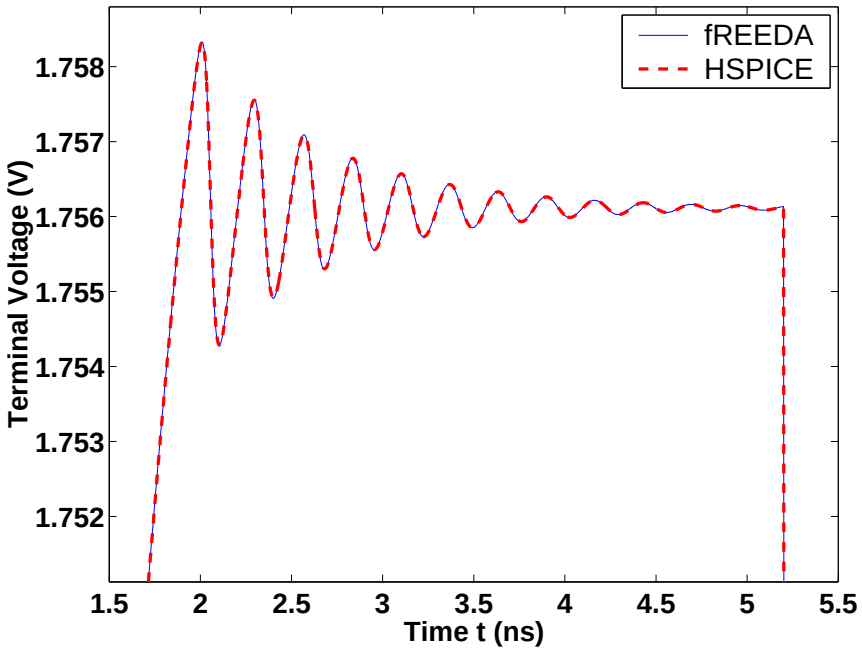

Figure 3.6: Transient analysis comparison of the terminal voltage

design of optoelectronic ICs.

The DHLD model is driven by a current pulse that has a peak value of 150 mA and a rise time of 0.1 ns and the simulations are presented for different values of β. The plots in Fig. 3.6 shows the input terminal voltage versus time while the plots in Fig. 3.7 shows the normalized output photon density. As we can see, a very small change in the input voltage correspond to a large ringing effect in the output power and this is due to exponential current/voltage relationship of the diode. Also, Fig. 3.7 shows the laser turn-on delay.

As shown in all of the plots, there is excellent agreement between *f*REEDA™ and HSPICE®.

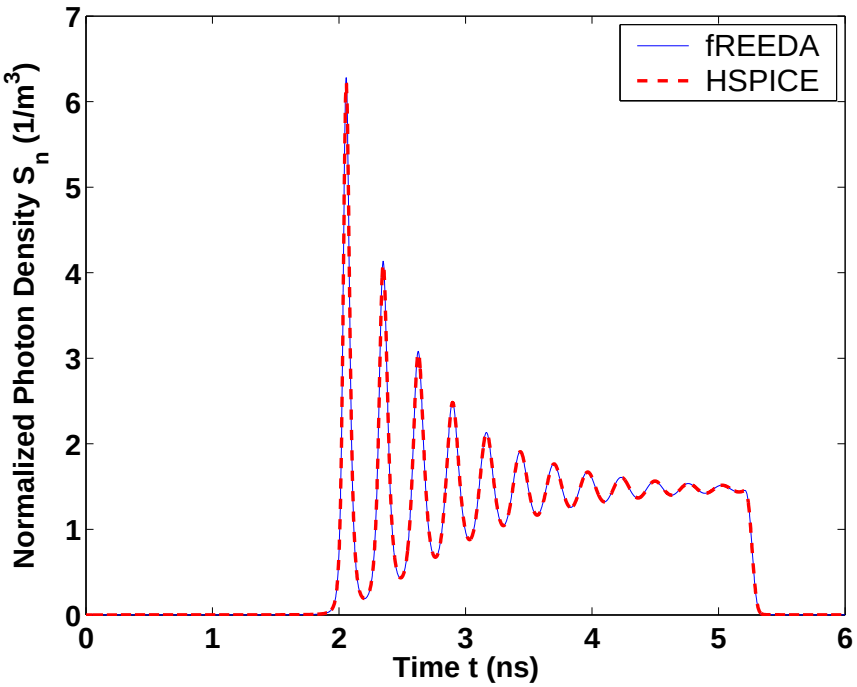

Figure 3.7: Transient Analysis comparison of the light output

3.5.2 Harmonic Balance

Fiber-optic microwave links have the potential to be used in a large number of applications such as cable television systems and personal communication systems. That is why it is important to characterize the behavior of the laser diode under direct microwave intensity modulation, and one of the most important tools in the simulations of nonlinear models at microwave frequencies is Harmonic Balance.

The laser diode was connected to the parasitics and matching network as shown in Fig. 3.8 and harmonic balance simulations with a single and two tone sine wave input were performed.

The intensity modulation response of a double heterojunction laser diode to an rf-input input power of 7 dBm at 1 GHz at a bias current of 125 mA was simulated. The time domain results are shown in Figs. 3.9 and 3.10 and compared to transient analysis. The calculated optical output power spectrum is shown in Fig. 3.11, with the second harmonic being approximately 7.59 dBc.

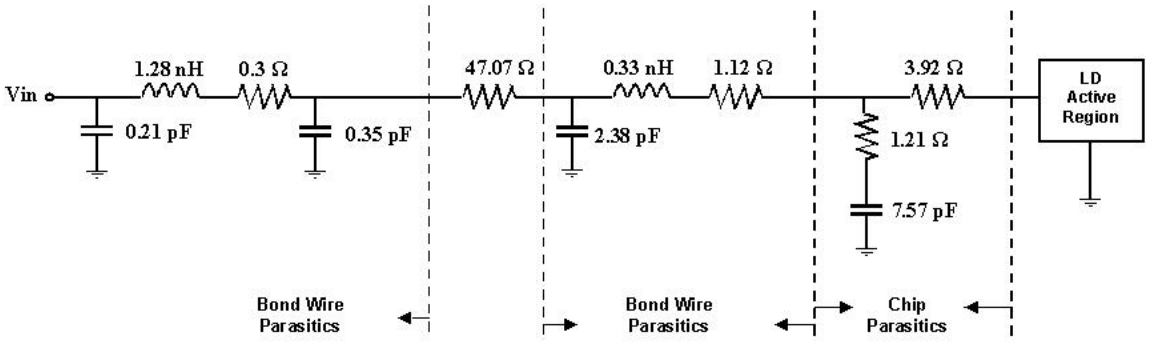

Figure 3.8: Parasitics and matching network used in HB simulation. After [17].

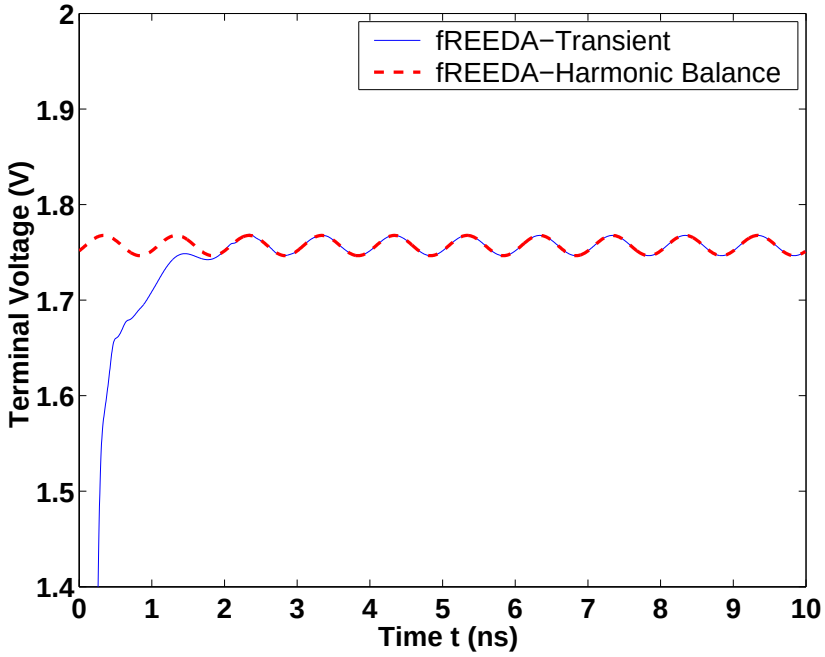

Figure 3.9: Comparison of the input terminal voltage between HB analysis and transient analysis in *f*REEDA™.

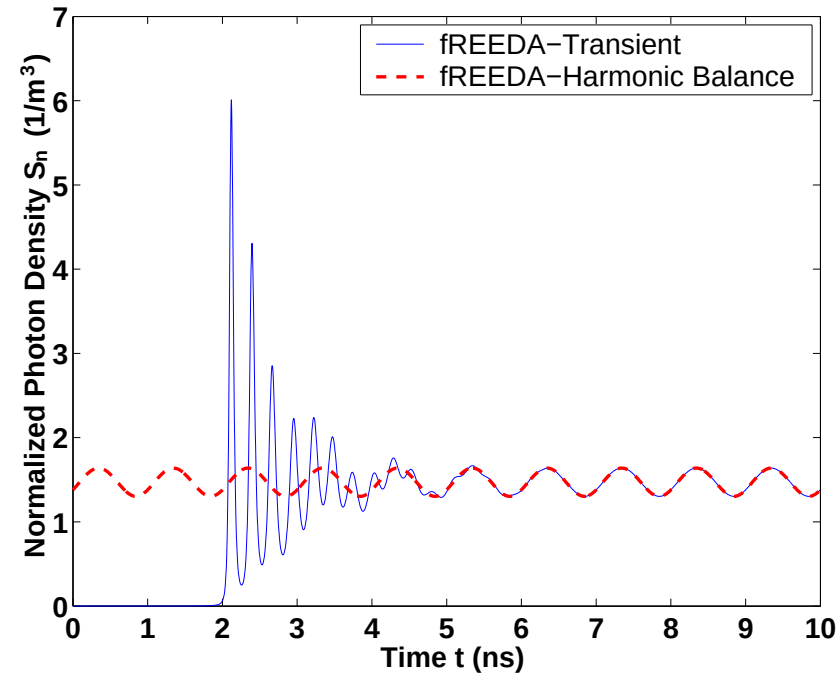

Figure 3.10: Comparison of the output photon density between HB analysis and transient analysis in *f*REEDA™.

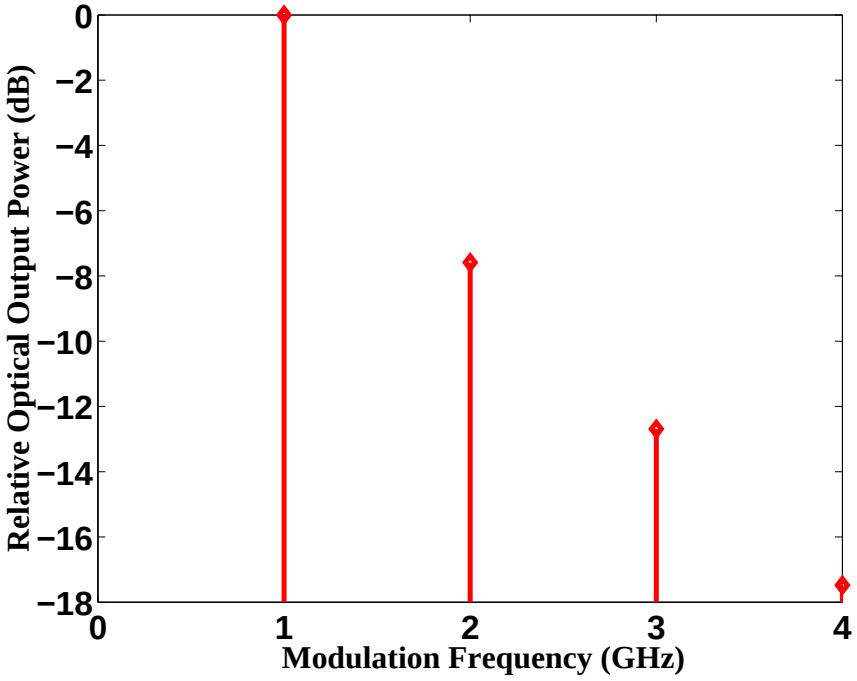

Figure 3.11: Large-signal intensity modulation response.

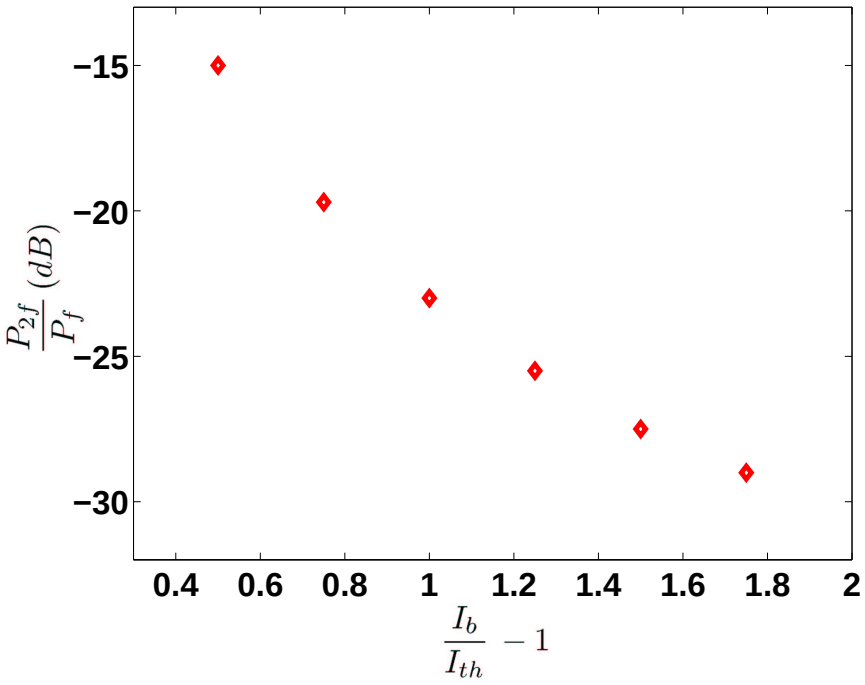

Figure 3.12: Power ratio of second harmonic to fundamental as a function of bias current.

Fig. 3.12 shows the power ratio of the second harmonic to the fundamental P_{2f}/P_f as a function of the bias current for an rf-input input power of 3 dBm at input frequency of 1 GHz. The threshold current of this device is 100 mA.

Finally, Fig. 3.13 shows the power ratio of the third-order intermodulation products to the carrier P_{IM3}/P_f as a function of the bias current. Equal inputs of -1 dBm at 1.0 GHz and 1.04 GHz were used. In general, there is an improvement in linearity with increasing bias current.

As we can see, there is an excellent agreement in the single tone simulations between HB and transient analysis except at the beginning with HB which truncates the transient response. In addition, the two tone simulations shows a close agreement with the reported nonlinear distortion simulations in the literature [17, 18].

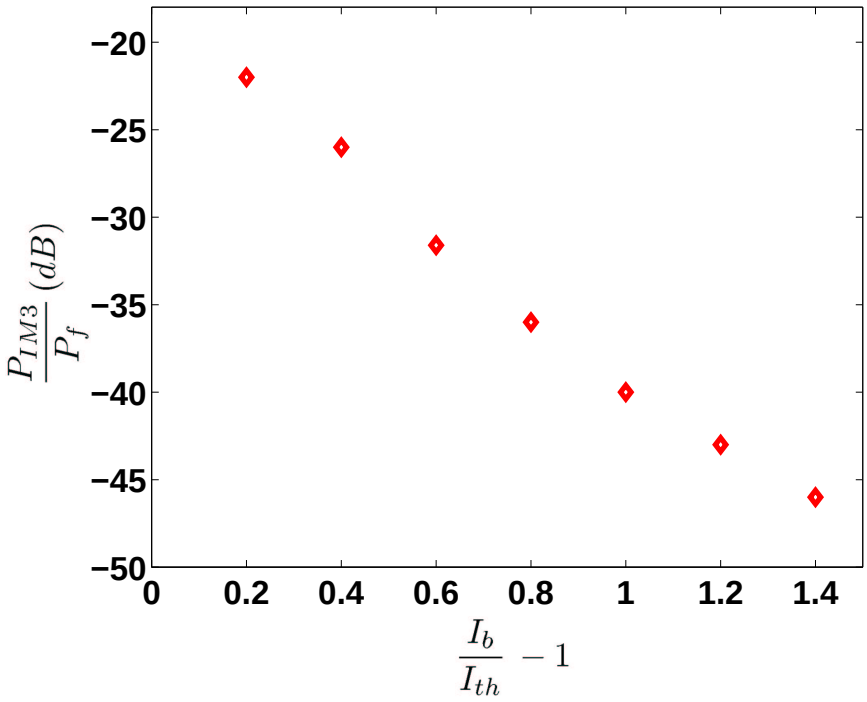

Figure 3.13: Power ratio of third-order intermodulation products to carrier as a function of bias current.

Chapter 4

The VCSEL Model

4.1 Introduction

Vertical-Cavity Surface-Emitting Lasers (VCSEL's) were first proposed by Prof. K. Iga of the Tokyo Institute of Technology in 1977 [19] and have attracted considerable interest in recent years due to the many advantages they offer compared to the edge-emitting semiconductor lasers. For example, they posses a single-longitudinal-mode of operation and a circular output beam. Also their planar structure, where the optical cavity is formed along the device's growth direction as shown in Fig. 4.1, results in many important advantages such as compatibility with on-wafer probing, and one and two-dimensional (1-D and 2-D) integration of VCSEL arrays. The laser diode analyzed here is an 863 nm bottom-emitting VCSEL with a 16 mm diameter, as described in [20]. The laser diode model is based on the simple thermal VCSEL model developed by Mena *et.al.* [21]. It is a semi-empirical model based on the standard laser rate equations and a thermally dependent empirical offset current. The following sections describes in details the governing equations of the model and its implementation in *f*REEDA™.

4.2 Parameter Table

Table 4.1 lists the parameters used to model the VCSEL Diode in *f*REEDA™.

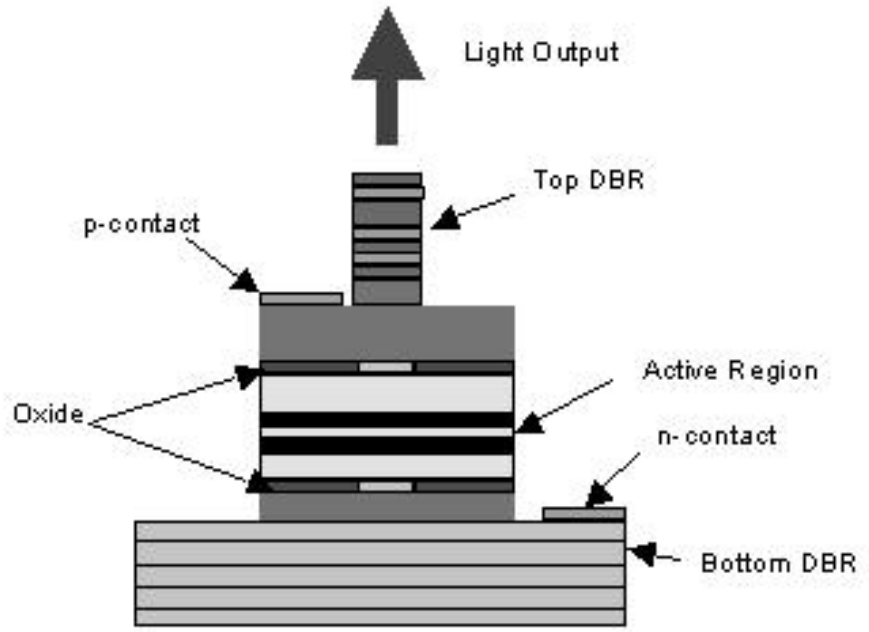

Figure 4.1: VCSEL Structure laser. After [22].

4.3 Analysis

One of the most recognized limitation of a VCSEL's performance is its thermal behavior. Due to the large electrical resistance introduced by the Distributed Bragg Reflector (DBR's) [21] and their poor heat dissipation characteristics, typical VCSEL's undergo relatively severe heating and consequently can exhibit strong thermally dependent behavior. That is why the effects of self heating on the output characteristics of VCSEL's are very significant. For example, thermal lensing can yield considerable differences between cw (continuous wave) and pulsed operation, as well as altering the emission profile of the laser's optical modes. However, the most important effect is exhibited in the device's static LI (light versus current) characteristics. First, as with edge-emitters, VCSEL's exhibit temperature-dependent threshold current. Also, because the active-region temperature increases severely with the injection current, cw operation is limited by a sharp roll-over in the output power [23].

Clearly, for any VCSEL model to be effective for the design of optoelectronic applications, the model should capture thermal effects, in particular the temperature-

Table 4.1: Parameters for the VCSEL Laser Diode Model

Parameters	**Description**	**Values**	**Units**
η_i	Injection Efficiency	1	-
β	Spontaneous Emission Coupling Coefficient	1e-6	-
τ_n	Carrier Recombination Lifetime	5e-9	s
k	Output coupling efficiency	2.6e-8	W
g_0	Gain Coefficient	1.6e4	s^{-1}
n_0	Carrier Transparency number	1.94e7	-
τ_p	Photon Lifetime	2.28e-12	s
a_0	1st temperature coefficient of the offset current	1.246e-3	A
a_0	2nd temperature coefficient of the offset current	-2.545e-5	A/K
a_1	3rd temperature coefficient of the offset current	2.908e-7	A/K^2
a_0	4th temperature coefficient of the offset current	-2.531e-10	A/K^3
a_1	5th temperature coefficient of the offset current	1.022e-12	A/K^4
ρ	Refractive index change	2.4e-9	-
n	Refractive Index	3.5	-
λ_0	Wavelength	863e-9	m
R_{th}	Thermal Impedance	2.6e3	$^oC/W$
τ_{th}	Thermal time constant	1e-6	s
T_0	Ambient Temperature	20	^oC

dependent threshold current and output power roll-over. Also, the model must be able to simulate both static and dynamic modulation of the laser. To meet the above criteria, the model should be based on temperature dependent rate equations. The strong thermal dependence of VCSEL's can be attributed to a number of mechanisms [21] such as Auger recombination and optical losses, however, the most important effects during static, or cw, operation are due to the temperature-dependent gain and carrier leakage out of the active region. For simplicity, the model in [21] ignores the temperature-dependence of the gain and the carrier leakage is taken into account by introducing a thermally dependent empirical offset current into the model equations.

The above threshold static LI characteristics of the VCSEL can be modeled using $P_o = \eta(T)(I - I_{th}(N,T))$, where P_o is the optical output power, $\eta(T)$ is the temperature dependent differential slope efficiency, I is the injection current, and $I_{th}(N,T)$ is the threshold current as a function of the carrier number N and the active region temperature T. Assuming that the temperature dependence of the differential slope

efficiency is minimal, and neglecting the effect of spatial hole burning [21], the output power expression becomes:

$$P_o = \eta(I - I_{th}(T)) \tag{4.1}$$

where $I_{th}(T)$ can be expressed as a constant value I_{tho} plus an empirical thermal offset current $I_{\text{off}}(T)$, that is $I_{th}(T) = I_{tho} + I_{\text{off}}(T)$. The temperature-dependent offset current could be a function of any form, but for simplicity, it is taken as a polynomial function of temperature

$$I_{\text{off}}(T) = a_0 + a_1 T + a_2 T^2 + a_3 T^3 + a_4 T^4 + \cdots \tag{4.2}$$

where the coefficient $a_0 - a_4$ can be determined during parameter extraction. It is important to note that because Eqn. 4.2 is not exclusively an increasing function of temperature, it should be able to capture the general temperature dependence of the VCSEL's LI curves.

Now that we have described a method to consider the thermal effect on the leakage current, we need an expression of the temperature characteristics of the VCSEL. While it is possible to adopt a numerical representation of a VCSEL's temperature profile as a function of the heat dissipation the device, a better method and more suitable for circuit level simulations is to describe the active region temperature via a thermal rate equation as follows [21]:

$$T = T_o + (IV - P_o)R_{th} - \tau_{th}\frac{dT}{dt} \tag{4.3}$$

where T_o is the ambient temperature, V is the terminal voltage of the laser, R_{th} is the VCSEL's thermal impedance which relates temperature change to the heat power dissipation, and τ_{th} is the thermal time constant which accounts to the nonzero response time of the device temperature (observed to be on the order of 1 μs [21]). Eqn. 4.3 also captures the thermal dynamics which is important in the transient characteristics of a VCSEL.

4.3.1 Rate Equations

As discussed before, the model should be able to simulate both static (DC) and dynamic (transient) modulation of the VCSEL. To do this, the model should be

based on the laser rate equations. Fortunately, the simple above-threshold LI curves described by $P_o = \eta(I - I_{th})$ can be described by the standard laser rate equations [24]. Thus, by introducing the empirical offset current $I_{\text{off}}(T)$ into these equations, the model should be able to simulate the LI curves of the VCSEL at different temperature as well as the dynamic behavior such as small-signal and transient modulation.

After the addition of the offset current, the laser rate equations become:

$$\frac{dN}{dt} = \frac{\eta_i(I - I_{off}(T))}{q} - \frac{N}{\tau_n} - \frac{G_o(N - N_o)S}{1 + \varepsilon S} \tag{4.4}$$

$$\frac{dS}{dt} = -\frac{S}{\tau_p} + \frac{\beta N}{\tau_n} + \frac{G_o(N - N_o)S}{1 + \varepsilon S} \tag{4.5}$$

where S is the photon number, N is the carrier number, N_o is the carrier transparency number, η_i is the injection efficiency, τ_n is the carrier recombination lifetime, G_o is the gain coefficient, τ_p is the photon lifetime, and β is the spontaneous emission coupling coefficient. As we can see, the introduction of the offset current into the rate equations is quite simple, however, it is an extremely effective means of describing the thermal dependence of the VCSEL's continuous wave LI characteristics. In addition, since the model is based on the rate equations, it should be able to simulate the non-dc behavior of the VCSEL. Finally, the optical output power is described using $P_o = kS$, where k is a scaling factor accounting for the output coupling efficiency of the laser.

4.3.2 Current/Voltage characteristics

The current-voltage relationship of the VCSEL can be expressed in great detail based on its diode-like characteristics, however, the voltage across the device in this model has been selected to be an arbitrary empirical function of current and temperature as follows:

$$V = f(I, T)\cdot \tag{4.6}$$

Then, the complete electrical characteristics of the VCSEL can be accounted for by introducing capacitors and other parasitics components in parallel with this voltage (in which case Eqn. 4.3 should be modified such that it depends on the total device current and not just I). The advantage of this approach is that since different VCSELs

have different IV characteristics, the specific form of Eqn. 4.6 can be determined on a device-by-device basis. For example, the IV relationship could be modeled as $V = IR_s + V_T \ln(1 + I/I_s)$ where R_s is a series resistance, I_s is the diode's saturation current, and V_T is the diode's thermal voltage which is usually temperature dependent. In other cases, a polynomial function of current and temperature [21] such as

$$V = (b_0 + b_1 T + b_2 T^2 + \cdots).(c_0 + c_1 I + c_2 I^2 + \cdots) \tag{4.7}$$

can be used, where b_n and c_n are constant parameters to be extracted. It is important to note that if experimental IV data is used to determine all the other parameters of the model first, then the exact form of Eqn. 4.6 can be determined at the very end of parameter extraction of a specific device. This approach actually has may advantages. First, it allows the voltage's current and temperature dependence to be accurately modeled. Second, it permits the optical and electrical characteristics to to be decoupled from one another, therefore simplifying the extraction of the model's parameters. For the VCSEL in consideration, the author provides only the IV characteristics at room temperature. That is why the IV data was fitted simply to a polynomial function of current as follows:

$$\begin{aligned} V &= 1.721 + 275I - 2.439 \times 10^4 I^2 + 1.338 \times 10^6 I^3 \\ &\quad -4.154 \times 10^7 I^4 + 6.683 \times 10^8 I^5 - 4.296 \times 10^9 I^6 \ . \end{aligned} \tag{4.8}$$

4.4 Implementation in fREEDA™

The large-signal model of the VCSEL follows from the rate equations, Eqn. 4.4 and Eqn. 4.5, from the temperature dependent offset current $I_{\text{off}}(T)$, from the thermal rate equation, Eqn. 4.3, and from the current/voltage characteristics of the diode described in Sec. 4.3.2. However, the implementation of the above equations as they are will lead to convergence problems and this is why variable transformation was used and the rate equations were normalized. First, S is transformed into a new variable X_s via $S = X_s/k$, and N into X_n via $N = z_n X_n$, where k is the output coupling efficiency and z_n is an arbitrary constants in the order of 10^7. This will

ensure that the state variables (X_s and X_n as discussed in the next section) will not take on very large values. Second, the rate equations were normalized so that every term in those equations is well behaved. That is, Eqn. 4.3 is divided by R_{th}, Eqn. 4.4 is multiplied by q/η_i and Eqn. 4.5 is multiplied by $\tau_p k$. The resulting equations are as follows:

$$\frac{T}{R_{th}} = \frac{T_o}{R_{th}} + (IV - P_o) - \frac{\tau_{th}}{R_{th}}\frac{dT}{dt} \tag{4.9}$$

$$\frac{qzn}{\eta_i}\frac{dX_n}{dt} = (I - I_{off}(T)) - \frac{qznX_n}{\eta_i \tau_n} - \frac{q}{\eta_i k}\frac{G_o(znX_n - N_o)X_s}{1 + \frac{\varepsilon}{k}X_s} \tag{4.10}$$

$$\tau_p \frac{dX_s}{dt} = -X_s + \frac{k\tau_p \beta znX_n}{\tau_n} + \frac{\tau_p G_o(znX_n - N_o)X_s}{1 + \frac{\varepsilon}{k}X_s} \tag{4.11}$$

Also, the model was modified to include the output wavelength λ which can be calculated from the carrier density N with the following equation [25]:

$$\lambda = \lambda_o[1 - \frac{\rho}{n}(N - N_o)] \tag{4.12}$$

where λ_o is the intrinsic band gap wavelength, ρ is the total variation of the refractive index due to the differences in injected current levels, and n is the refractive index of the medium.

To implement the model, we start by identifying the state variables, then by writing the model equations as a function of those state variables and their derivatives. Since the terminal voltage V is expressed in Eqn. 4.8 as a function of the current I (which could be the input terminal current or not depending on wether a parasitic capacitor C_l is included or not), I is chosen as the first state variable. Then, if C_l is not included, V can be directly written as a function of I. On the other hand, if C_l is included, then the total input current is expressed as $I_{tot} = I + I_{Cl}$ where $I_{Cl} = C_l dV/dt$ and can be expressed as:

$$I_{Cl} = C_l(c_1 + 2c_2 I + 3c_3 I^2 + 4c_4 I^3 + 5c_5 I^4)\cdot \tag{4.13}$$

Second, the three rate equations, Eqn. 4.9, 4.10, and 4.11, need to be satisfied. This is done by first augmenting the model with three ports (three terminals with their respective local reference terminals), second by letting the above equations be equal to the current at each of the respective port, and finally forcing that current

to zero by connecting an open circuit to that port. It is very much in the same way Eqn. 3.27 was satisfied as described in Sec. 3.4.

Finally, the voltage at the designated optical output power is described by $P_o = (v_m + \delta)$ where the current is meaningless. The same should also be done for implementing Eqn. 4.12.

4.5 Simulations and Results

The purpose of the following sections is to present some of the results of the VCSEL model implemented in *f*REEDA™.

In Sec. 4.5.1, a DC analysis is performed on the implemented VCSEL model. Graphs of the IV and LI curves at different ambient temperature are shown and compared to the measurments. Also, plots of the carrier number, output wavelength, and active region temperature versus the input current are presented.

Sec. 4.5.2 presents the results of the transient analysis. The model is driven by an input current pulse of finite rise and fall time. All the transient simulations are carried out at 20 ^{o}C ambient temperature. Graphs of the carrier number and active region temperature versus time are presented. Also, plots of the optical output power and wavelength chirp are shown.

In Sec. 4.5.3 a Harmonic Balance simulation is performed on the implemented VCSEL model. First, the frequency response of the VCSEL for an input rf power of –8 dBm is presented. Second, plots of the large signal wavelength chirp for different bias current is presented. Finally, the power ratio of the second harmonic to the fundamental P_{2f}/P_f and of the intermodulation distortion to the fundamental P_{IM3}/P_f as a function of bias current and temperature are shown.

The source code that implements the model, which consists of a C++ source file and a header file, can be found in Appendix B. The *f*REEDA™ netlists which was used to generate the plots in the following sections can be found in Appendix C.2.

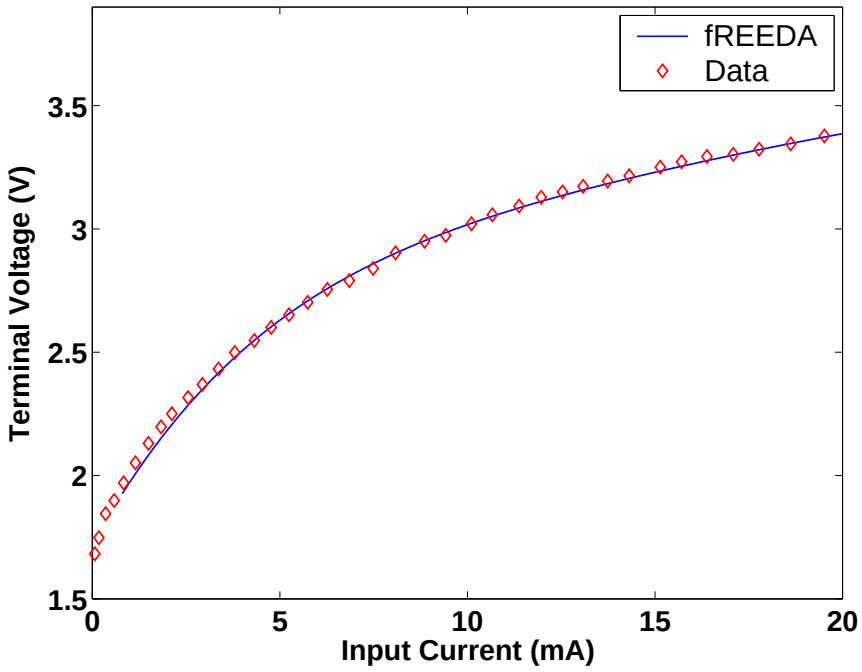

Figure 4.2: DC Analysis comparison of the IV curve of the VCSEL model and the measurement. Measurements from [21].

4.5.1 DC Analysis

The input terminal current is varied from 0 mA to 37 mA and the simulation is run at 3 different ambient temperature, 20 ^{o}C, 60 ^{o}C, and 100 ^{o}C. Fig. 4.2 shows the IV curve of the VCSEL (only one curve is show since the IV characteristics of the diode is modeled as an independent function of temperature).

Plots in Fig. 4.3 shows a family of curves of the carrier number in the active region as a function of the input current at different ambient temperature. From this graph, we can clearly deduce two things. First, and as expected, the carrier number will not increase anymore once threshold is reached. Second, carrier leakage starts at a much lower input current at high ambient temperature. Also, as seen in Fig. 4.4, the wavelength is constant above threshold. This is due to the fact that the output wavelength is mainly a function of the carrier number. Finally, Fig. 4.5 shows the plots of the active region temperature versus the input current for different ambient temperature. It is clear from these plots how severely the VCSEL can be heated.

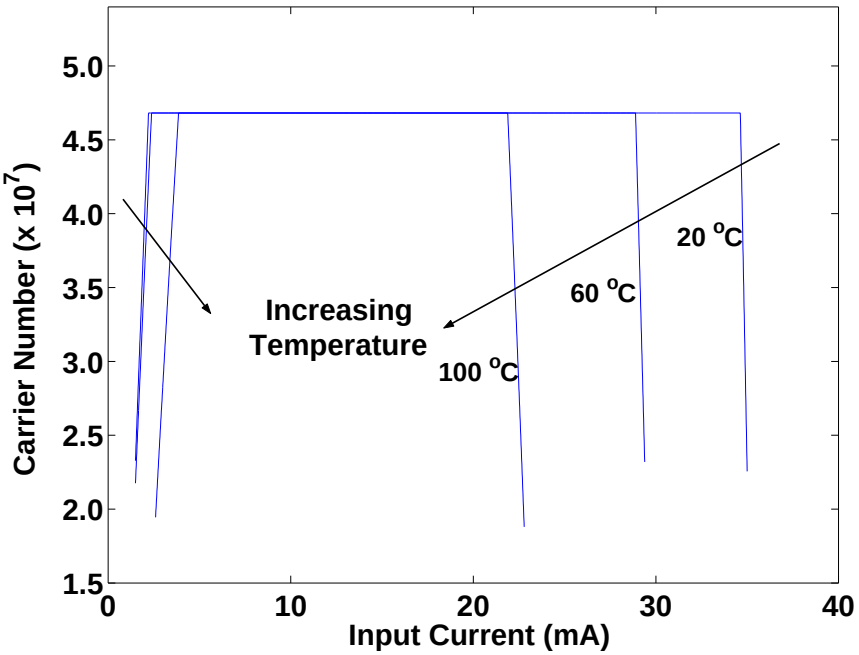

Figure 4.3: DC Analysis plots of the carrier number at different ambient temperature.

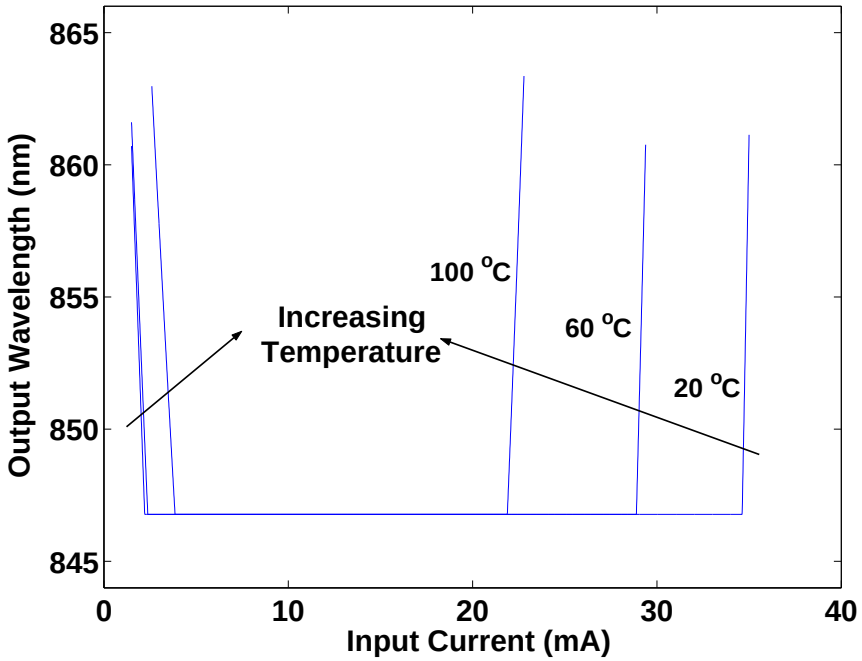

Figure 4.4: DC Analysis plots of the output wavelength at different ambient temperature.

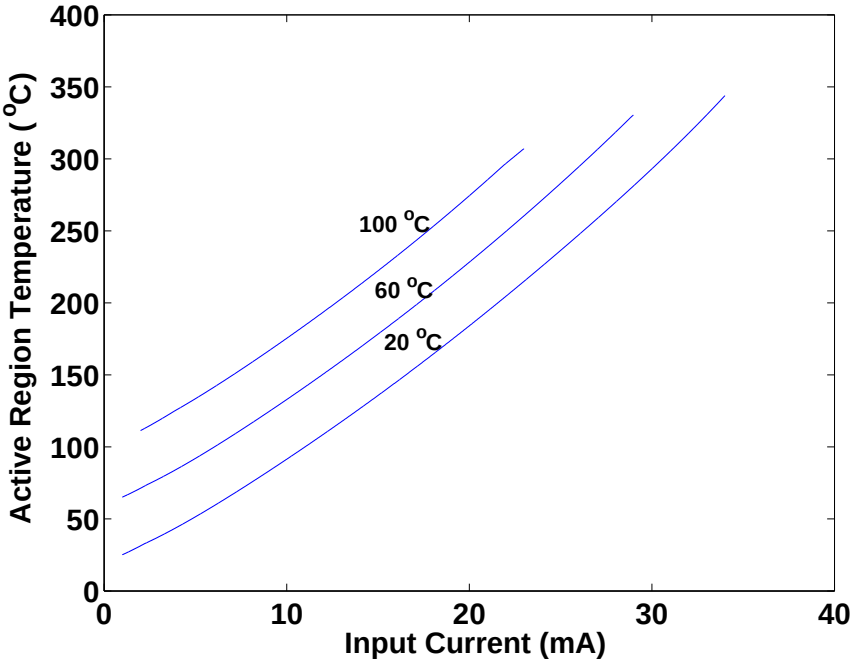

Figure 4.5: DC Analysis plots of the active region temperature increase at different ambient temperature.

The optical output power as a function of the input current is shown in Fig. 4.6. From these plots, we can deduce a lot of things. First, there is a threshold current shift at different ambient temperatures. In addition, there is a significant reduction in the slope efficiency and the maximum output power. Finally, the effect of carrier leakage is obvious and manifest itself clearly in the optical output roll over and the complete turn-off of the laser.

As we can see in the IV and LI plots, there is an excellent agreement between the simulations in *f*REEDA™ and the measurments.

4.5.2 Transient Analysis

While DC simulations are very important to identify key factors such as threshold current, maximum output power and temperature effects in the VCSEL, transient analysis is also a crucial part in the design of OEICs. This is the main reason why the model was based on the laser rate equations.

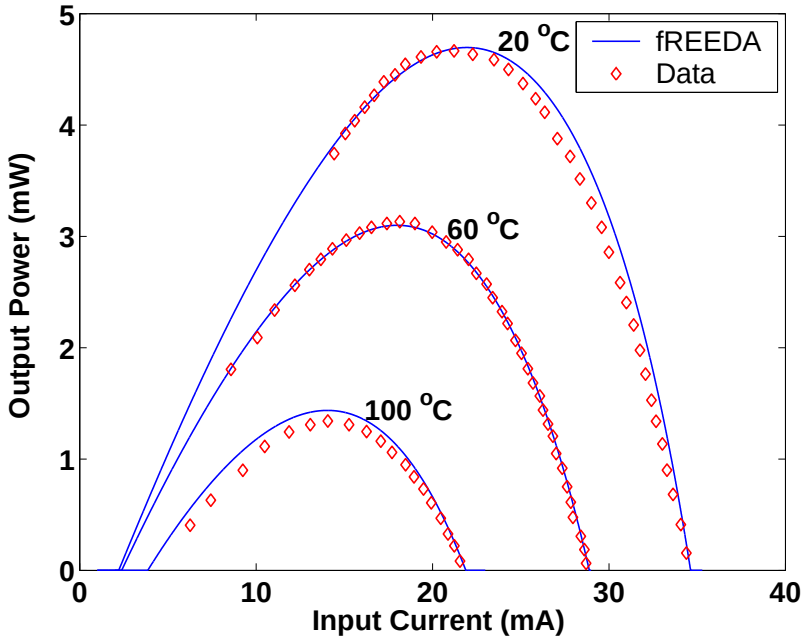

Figure 4.6: DC Analysis comparison of the LI curves at different ambient temperature with the measurement. Measurements from [21].

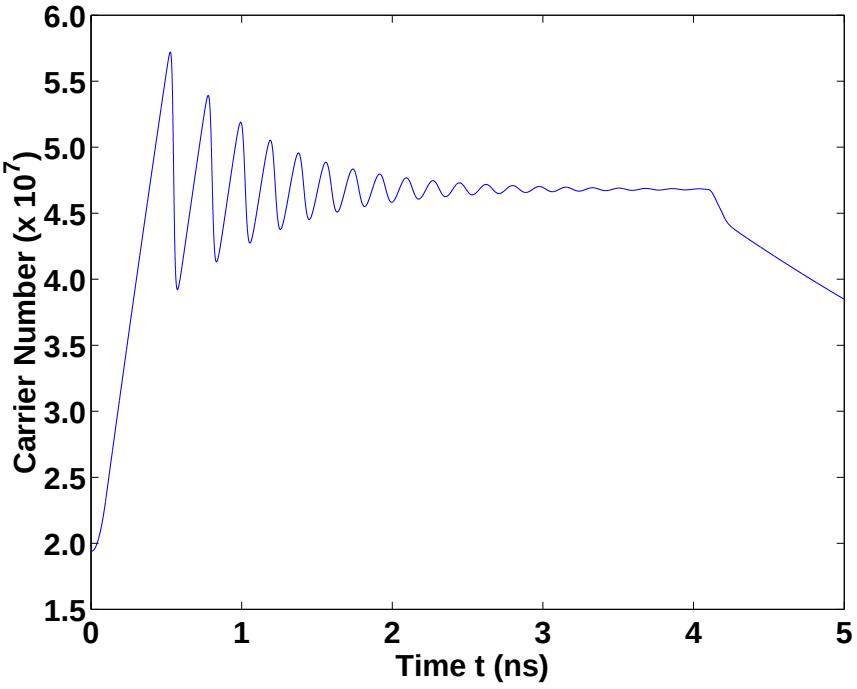

Figure 4.7: Transient analysis plot of the carrier number at 20 ^{o}C.

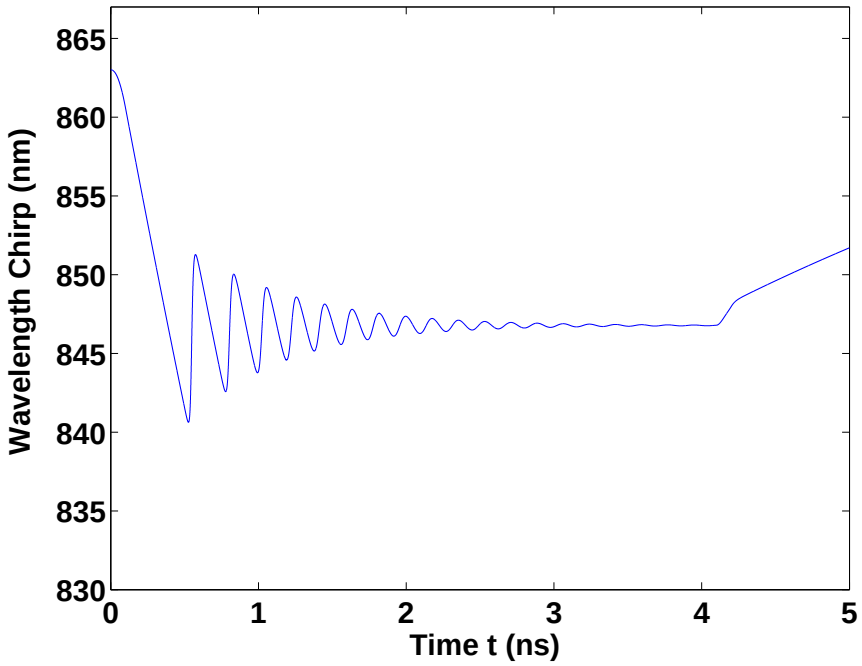

Figure 4.8: Transient analysis plot of the wavelength chirp at 20 ^{o}C.

The VCSEL is driven by a current pulse that has a peak value of 15 mA, a period of 5 nano-seconds, and a rise and fall time of 0.1 ns. The ambient temperature is set to 20 ^{o}C during the simulations. The plots in Fig. 4.7 show the carrier number versus time while Fig. 4.8 shows the plots of wavelength chirp which is a critical factor in the design of Wavelength Division Multiplexed (WDM) Systems. Fig. 4.9 shows how fast is the increase in the active region temperature and plots in Fig. 4.10 shows the optical output power. In the last figure, the optical output power shows the well known laser turn-on delay and ringing effects.

4.5.3 Harmonic Balance

VCSEL diodes are promising light sources for low-cost, high-performance optical microwave links in microcellular networks and high speed phased-array radar antenna [27]. Lately, analog fiber-optic link based on directly modulated VCSELs was also proposed to get rid of the digital data transmission limitations in hazardous highly radioactive environment with large temperature variation from 50 to 200 ^{o}C

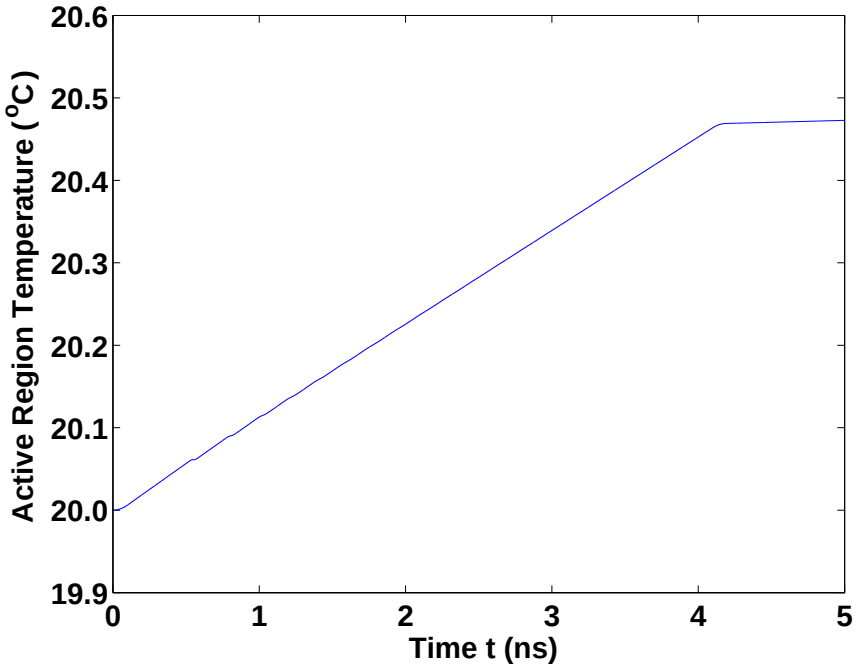

Figure 4.9: Transient analysis plot of the increase in the active region temperature at 20 ^{o}C.

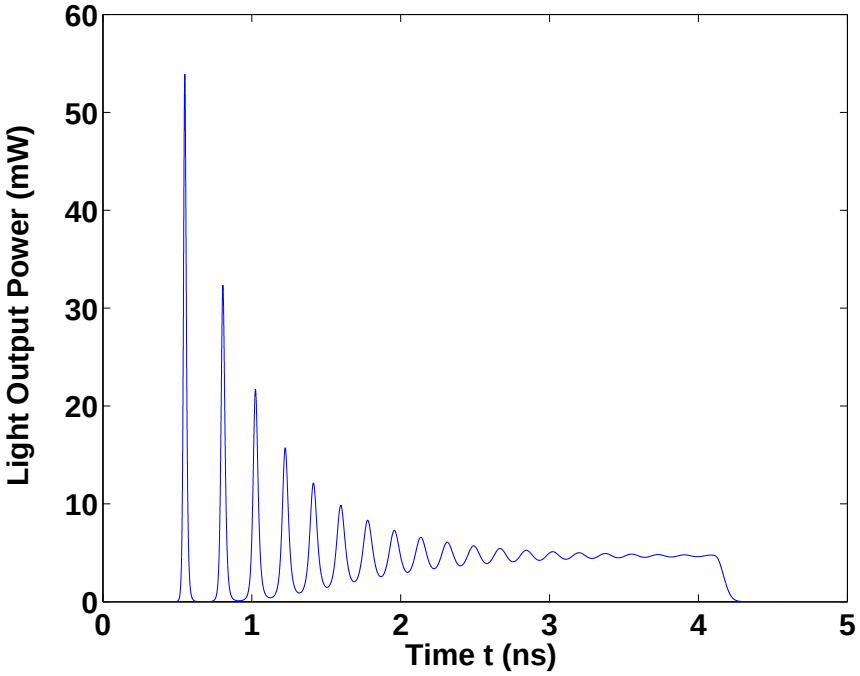

Figure 4.10: Transient analysis plot of the output optical power at 20 ^{o}C.

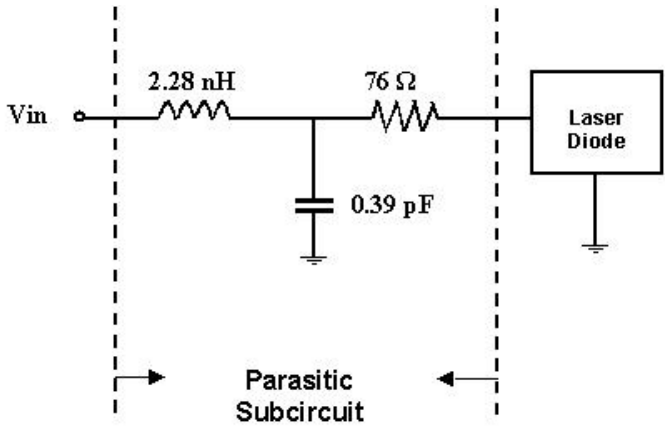

Figure 4.11: Parasitic network used in HB simulation. After [26].

such as thermonuclear reactors [28]. It is therefore of great importance to characterize the VCSEL's behavior for analog applications at microwave frequencies.

In this section, Harmonic Balance was used to study the VCSEL's characteristics of importance to microwave modulation such as the modulation response, the large signal wavelength chirp, and most importantly the VCSEL's linearity as a function of bias current and ambient temperature. First, the laser was connected to the parasitic network shown in Fig. 4.11 and the VCSEL's harmonic response was characterized. The laser was driven by a single tone rf-input power of –8 dBm and the amplitude of the first three harmonic peaks were monitored as the signal frequency was varied. Fig. 4.12 shows the modulation response of the VCSEL at a bias current of 12 mA while Fig. 4.13 and 4.14 are the plots at a bias current of 14 mA and 16 mA respectively. As we can see, the first-order relaxation resonance frequency appears to be around 4 GHz and shifts towards 5 GHz at higher bias current. Also, the laser appears extremely nonlinear at this high input power specifically around the resonant frequency.

Fig. 4.15 shows the large signal wavelength chirp as the input frequency was varied at different bias current. The plots shows that the wavelength chirp increases with increasing bias current and it peaks at the resonant frequency.

Second, the VCSEL was driven by a single tone RF-input signal of –20 dBm

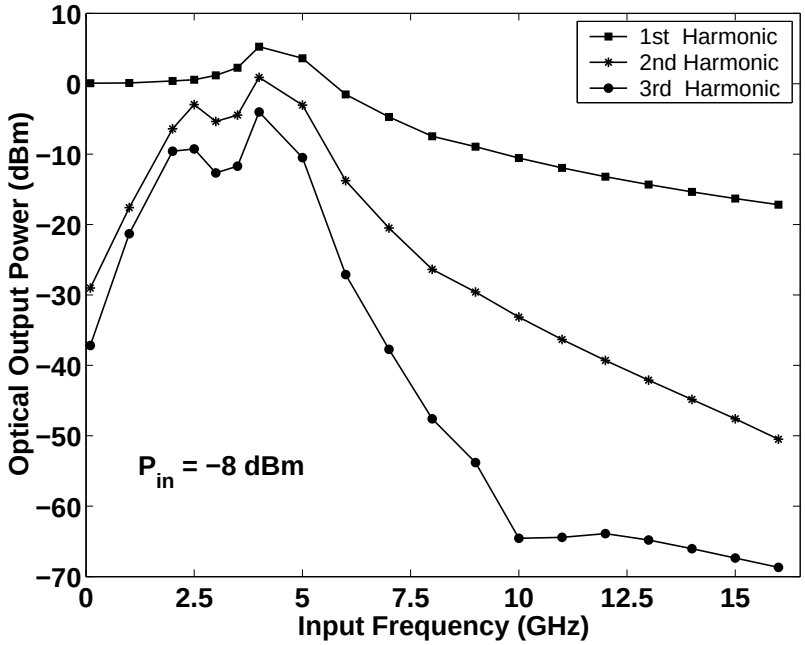

Figure 4.12: Frequency response of the first three harmonics for a constant input signal power of –8 dBm at 12 mA bias current.

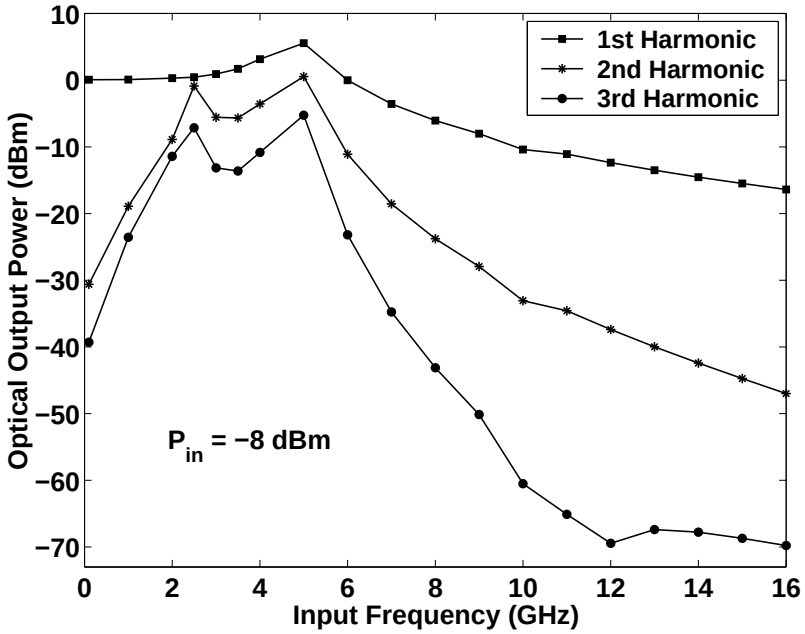

Figure 4.13: Frequency response of the first three harmonics for a constant input signal power of –8 dBm at 14 mA bias current.

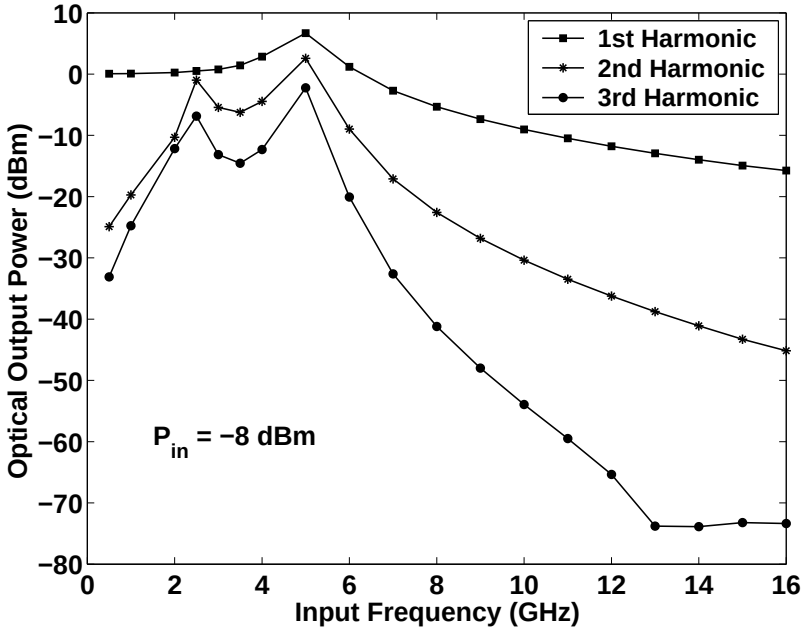

Figure 4.14: Frequency response of the first three harmonics for a constant input signal power of –8 dBm at 16 mA bias current.

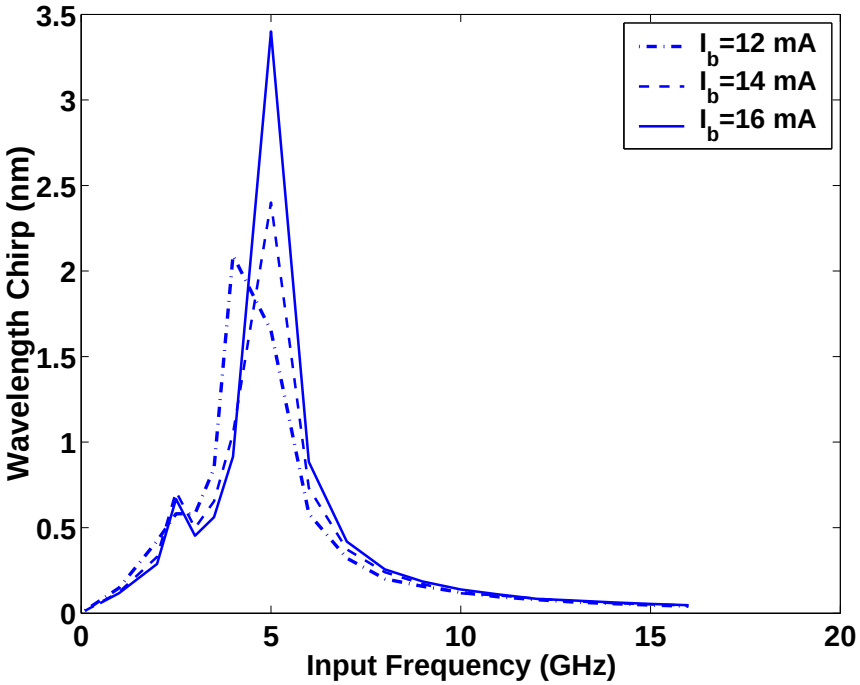

Figure 4.15: Plots of the wavelength chirp versus frequency at different bias current.

at 1 GHz. Fig. 4.16 shows plots of the power ratio of the second harmonic to the fundamental P_{2f}/P_f as a function of bias current at different ambient temperature. The results shows that there is an increase in linearity with bias current up to the power rollover point where linearity starts to decrease again. It is also interesting to see this linearity level given the nonlinear LI curves of the laser (Fig. 4.6) and that the VCSEL is mostly linear around the maximum output power bias point. However, the VCSEL's linearity decreases considerably with increasing ambient temperature and this could be explained by the fact that at higher ambient temperature, the same input RF power will drive the VCSEL more into the off region leading to more harmonic distortion.

Finally, the VCSEL was driven by two signals of equal input power of -20 dBm at 1.0 GHz and 1.01 GHz. Fig. 4.17 shows the power ratio of the third-order intermodulation product to the carrier P_{IM3}/P_f as a function of the bias current at different ambient temperature. Again, the results shows that the VCSEL's nonlinear behavior is similar to the results described in the previous figure.

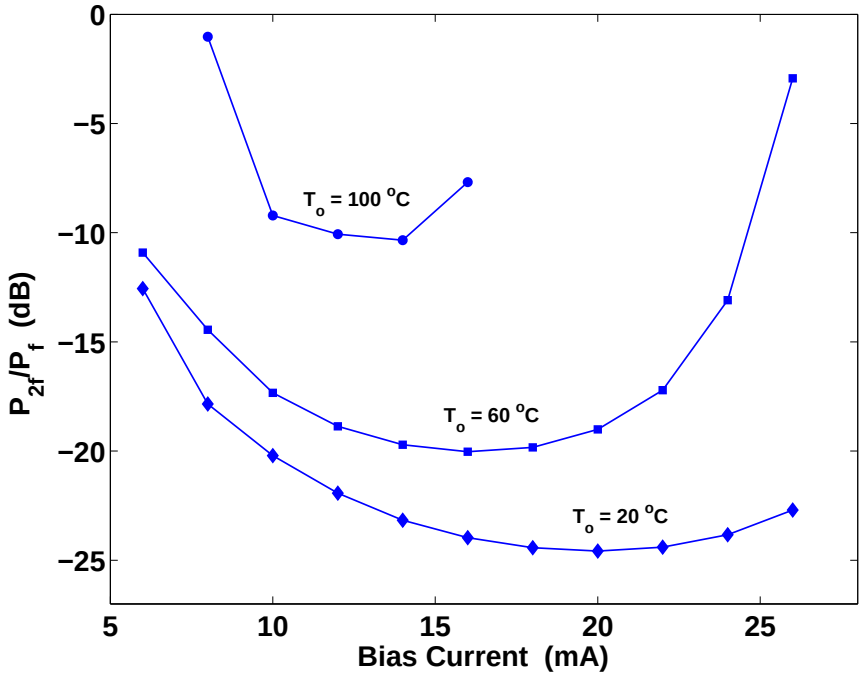

Figure 4.16: Power ratio of second harmonic to fundamental as a function of bias current for different temperature.

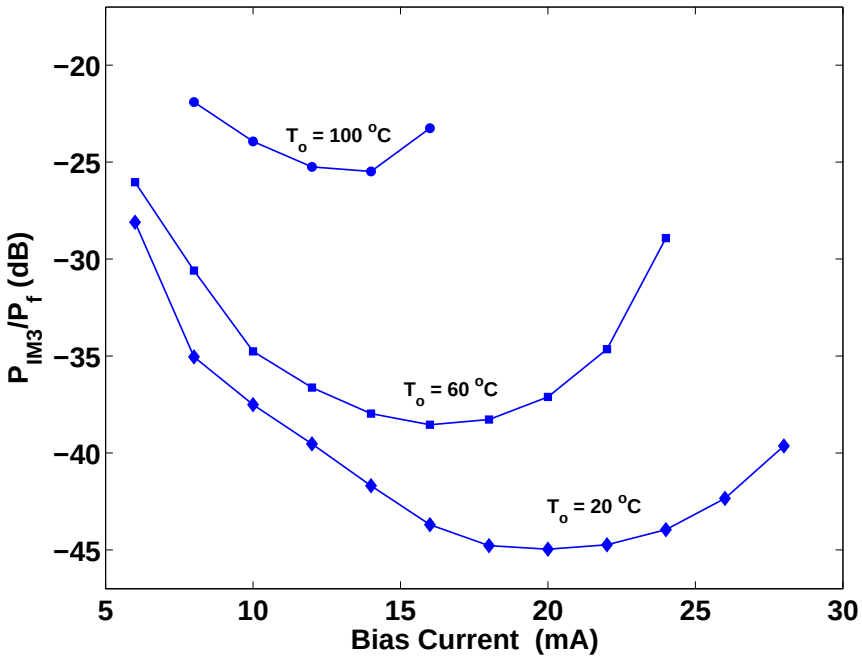

Figure 4.17: Power ratio of third-order intermodulation products to carrier as a function of bias current for different temperature.

Chapter 5

Conclusions and Future Research

5.1 Conclusions

Two laser diode model, of a DH and a VCSEL, were successfully implemented in *f*REEDA™ and its state variable formulation and object oriented design was found to offer a great flexibility and conciseness. The C++ source code consisted of just two files, a header file and a source file where the actual coding of the equations in both models were just a little bit above one page. In both models, parameterization and variable transformation were used to insure better convergence and numerical stability.

For the DH diode, the models was tested with transient and Harmonic Balance simulations and the results shows an excellent agreement with HSPICE® (in case of transient analysis) and reported nonlinear distortion simulations in the literature. For the VCSEL diode, the models was tested with DC, transient, and Harmonic Balance simulations and the DC simulations shows an excellent agreement with the measurments.

In both models, the implementation in *f*REEDA™ was fast, simple and with almost behavioral-like coding. Also, the same code is used with different analysis type *i.e.* DC, Transient, and Harmonic Balance. With its OO-design, its ability to capture true

time delay, and its universal device modeling capability, fREEDA™ is an efficient tool that can be used for fast prototyping and modeling of laser diodes and optoelectronic devices.

5.2 Future Research

There are many interesting directions and future research for laser diode and packaged optoelectronic model development in fREEDA™ . Some of them are:

- Implementation of VCSEL models that is suitable for the simulations of packaged VCSEL arrays. That is, the model should not only takes into account the intrinsic thermal behavior of an isolated VCSEL, but should also include thermal cross-talk of neighboring ones.

- Incorporating optical feedback into the models and study its effect on turn-on delay and linearity performance. This can be done in fREEDA™ with its ability to keep track of true time delayed state-variables in conjunction with being able to run both transient and harmonic balance simulations.

- Modeling of electrical packaging effects in VCSELs and optoelectronic devices. This is done in fREEDA™ with its implementation of the local reference terminal concept that allows the incorporation of electromagnetic models in the circuit simulator.

Bibliography

[1] N. Bewtra, D. A. Suda, G. L. Tan, F. Chatenoud, and J. M. Xu, "Modeling of Quantum-Well Lasers with Electro-Opto-Thermal Interaction," *IEEE J. of Selected Topics in Quantum Electronics*, Vol. 1, No. 2, pp. 331-340, June 1995.

[2] J. Morikuni, G. Dare, P. Mena, A. Harton, K. Wyatt, "Simulation of optical interconnect devices, circuits, and systems using analog behavioral modeling tools," *IEEE Lasers and Electro-Optics Society Annual Meeting*, Vol. 1, pp. 235–236, Dec 1998.

[3] *http://www.freeda.org.*

[4] A. Griewank, D. Juedes and J. Utke, "Adol-C: A Package for the Automatic Differenciation of Algorithms Written in C/C++" ACM TOMS, Vol. 22(2), pp. 131-167, June 1996.

[5] J. Hecht, "Laser Pioneers" *Boston: Academic Press*, 1992.

[6] R. D. Dupuis "An Introduction to the Developement of the Semiconductor Laser" *IEEE J. of Quantum Electronics*, Vol. QE-23, No. 6, June 1987.

[7] J. Morikuni, P. Mena, A. Harton, K. Wyatt, "Optoelectronic Computer-Aided Design," *IEEE Lasers and Electro-Optics Society Summer Topical Meetings*, pp. 53–54, July 1998.

[8] L. Seung-Woo, C. Eun-Chang, C. Woo-Young, "Optical interconnection system analysis using SPICE, " *The Pacific Rim Conference on Lasers and Electro-Optics*, Vol. 2, pp. 391–392, Sep 1999.

[9] C. E. Christoffersen, *Global Modeling of Nonlinear Microwave Circuits*, Ph.D. Dissertation, Dept. of Electrical Engineering, North Carolina State University, 2001.

[10] W. B. Joyce, R. W. Dixon, "Electrical characterization of heterostructure lasers," *in J. Appl. Phys.*, Vol. 49, No. 7, July 1978.

[11] R. S. Tucker, "Circuit model of double-heterojunction laser below threshold," *in IEE Proc. on Solid-State & Electron Devices–Part I*, Vol. 128, No. 3, pp. 101–106, 1981.

[12] R. S. Tucker, "Large-signal circuit model for simulation of injection-laser modulation dynamics," *in IEE Proc. on Solid-State & Electron Devices–Part I*, Vol. 128, No. 5, pp. 180–184, 1981.

[13] H.C. Casey, M.B. Panish, "Heterosructure Lasers, part A and part B" *Academic Press*, 1978.

[14] L.A. Coldren, S.W. Corzine, "Diode Lasers and Photonic Integrated Circuits," *John Wiley & Sons, Inc.*, 1995.

[15] V. Rizzoli, A. Lipparini, A. Costanzo, F. Mastri, C. Cecchetti, A. Neri, D. Masotti, "State-of-the-art harmonic-balance simulation of forced nonlinear microwave circuits by the piecewise technique," *IEEE Transactions on Microwave Theory and Techniques*, Vol. 40, issue 1, pp. 12–28, Jan. 1992.

[16] S. N. Velu, *Charge Based Modeling in State Variable Based Simulator*, M.S. Thesis, Dept. of Electrical Engineering, North Carolina State University, 2002.

[17] W. I. Way, "Large Signal Nonlinear Distortion Prediction for a Single-Mode Laser Diode Under Microwave Intensity Modulation," *IEEE J. of Lightwave Technology*, Vol. LT-5, No. 3, March 1987.

[18] S. Iezekiel, C. M. Snowden, "Nonlinear Circuit Analysis of Laser Diodes Under Microwave Direct Modulation," *IEEE MTT-S International*, Vol. 2, pp. 937–940, 1990.

[19] E. Towe, R. F. Leheny, A. Yang, "A Historical Perspective of the Developement of the Vertical-Cavity Surface-Emitting Laser," *IEEE J. on Selected Topics in Quantum Electronics*, Vol.6, No. 6, Nov/Dec 2000.

[20] Y. Ohiso, K. Tateno, Y. Kohama, A. Wakatsuki, H. Tsunetsugu, and T. Kurokawa, "Flip-chip bonded 0.85-μm bottom-emitting vertical-cavity laser array on an AlGaAs substrate," *IEEE Photon. Technol. Lett.*, Vol. 8, pp. 1115-1117, Sep 1996.

[21] P. V. Mena, J. J. Morikuni, S.-M. Kang, A. V. Harton, K. W. Wyatt, "A Simple Rate-Equation-Based Thermal VCSEL Model," *IEEE J. of Lightwave Technology*, Vol. 17, No. 5, May 1999.

[22] M. A. Neifeld (private communication), 2003.

[23] G. Hasnain, K. Tai, L. Yang, Y. H. Wang, R. J. Fisher, J. D. Wynn, B. Weir, N. K. Dutta, and A. Y. Cho, "Performance of Gain-guided Surface Emitting Lasers with Semiconductor Distributed Bragg Reflectors," *IEEE J. of Quantum Electron.*, Vol. 27, No. 6, pp. 1377-1385, 1991.

[24] G. P. Agrawal, and N. K. Dutta, "Semiconductor Laser, 2nd ed." *New York: Van Nostrand Reinhold*, 1995.

[25] M. A. Neifeld and W. C. Chou, "Electrical packaging impact on source components in optical interconnect," *IEEE Transactions on Components, Packaging, and Manufacturing Technology — Part B*, Vol. 18, pp. 578–595, Aug. 1995.

[26] M. Bruensteiner, G. C. Papen, "Extraction of VCSEL Rate-Equation Parameters for Low-Bias System Simulation," *IEEE J. of Selected Topics in Quantum Electron*, Vol. 5, No. 3, 1999.

[27] C. Carlsson, H. Martinsson, R. Schatz, J. Halonen, A. Larsson "Analog Modulation Properties of Oxide Confined VCSELs at Microwave Frequencies," *IEEE J. of Lightwave Technology*, Vol. 20, No. 9, September 2002.

[28] A. F. Fernandez, F. Berghmans, B. Brichard, M. Decreton, "Toward The Developement of Radiation-Tolerant Instrumentation Data Links for Thermonuclear Fusion Experiments," *IEEE Transactin on Nuclear Science*, Vol. 49, No. 6, December 2002.

Appendix A

Double-Heterojunction Laser Diode Source Code

Section A.1 & A.2 contains the C++ code of the representation of the model in *f*REEDA™ . Section A.3 present the HSPICE® netlist.

A.1 The Header file, DHLD.h

```
// This may look like C code, but it is really -*- C++ -*-
//
// This is a Double Heterojunction laser Diode model (The R. S. Tucker model)
//
//               Laser Diode
//
//              ++++++++++++++
//              +             +
//          o---------        -----o
//              +    |        +
//              +  -----      +
//              +  \   /      +
//              +   \ /       +
//              +   ---       +
//              +    |        +
//          o---------        -----o
//       "gnd"  +             +   "oref"
//              ++++++++++++++
```

```
//
// by Houssam Kanj

#ifndef DHLD_h
#define DHLD_h 1

#include "../network/AdolcElement.h"

class DHLD : public AdolcElement
{
public:

  DHLD(const string& iname);

  ~DHLD() {}

  static const char* getNetlistName()
  {
    return einfo.name;
  }

  virtual void init() throw(string&);
   virtual void getLocalRefIdx(UnsignedVector& local_ref_vec,
                  TerminalVector& term_list);//


private:

  virtual void eval(adoublev& x, adoublev& vp, adoublev& ip);

  // Some constants
  double Vpara;  // like V1 in V. Rizzoli
  double vt, q;


  // Element information
  static ItemInfo einfo;

  // Number of parameters of this element
  static const unsigned n_par;

  // Parameter variables
```

```
  double rs, re, i01, i02, b, tns, c0, vd, d, a, rp, cp, sc, beta;

  // Parameter information
  static ParmInfo pinfo[];

};

#endif
```

A.2 The C++ source code file, DHLD.cc

```
#include "../network/ElementManager.h"
#include "../analysis/FreqMNAM.h"
#include "../analysis/TimeMNAM.h"
#include "DHLD.h"

// Static members
const unsigned DHLD::n_par = 14;

// Element information
ItemInfo DHLD::einfo = {
  "dhld",
  "Double Heterojunction Laser Diode",
  "Houssam Kanj",
  DEFAULT_ADDRESS"elements/DHLD.h.html"
};

// Parameter information
ParmInfo DHLD::pinfo[] = {
  {"rs", "Series Resistance value (Ohms)", TR_DOUBLE, false},
  {"re", "Nonlinear Series Resistance value (Ohms)", TR_DOUBLE, false},
  {"i01", "Equivalent Diode1 Saturation Current (Ampere)", TR_DOUBLE, false},
  {"i02", "Equivalent Diode2 Saturation Current (Ampere)", TR_DOUBLE, false},
  {"b", "Current Controlled Current Source gain (1/Ampere)", TR_DOUBLE, false},
  {"tns", "Equivqlent Reconbination Lifetime (Sec)", TR_DOUBLE, false},
  {"c0", "Zero-Bias Capacitance (Farad)", TR_DOUBLE, false},
  {"vd", "Diode Built-in potential (Volt)", TR_DOUBLE, false},
  {"d", "Constant relate the radiative recombination current per unit volume
   to the optical gain (meter^6/Ampere/Volt)", TR_DOUBLE, false},
  {"a", "nonradiative recombination lifetime/(nonradiative recombination
   lifetime + low level injection spontaneous recombination lifetime)
   = tn/(ts+tn)", TR_DOUBLE, false},
  {"rp", " --- (Ohms)", TR_DOUBLE, false},
  {"cp", " --- (Farad)", TR_DOUBLE, false},
  {"sc", "Photon density normalisation constant (meter^-3)", TR_DOUBLE, false},
  {"beta", "fraction of spontaneous emission coupled into the lasing mode",
   TR_DOUBLE, false}

};
```

```
DHLD::DHLD(const string& iname) : AdolcElement(&einfo, pinfo, n_par, iname)
{
  // Set default parameter values
  paramvalue[0] = &(rs = 2);
  paramvalue[1] = &(re = 0.468);
  paramvalue[2] = &(i01 = 2.54e-25);
  paramvalue[3] = &(i02 = 18.13e-3);
  paramvalue[4] = &(b = 6.92);
  paramvalue[5] = &(tns = 2.25e-9);
  paramvalue[6] = &(c0 = 10e-12);
  paramvalue[7] = &(vd = 1.65);
  paramvalue[8] = &(d = 1.79e-29);
  paramvalue[9] = &(a = 0.125);
  paramvalue[10] = &(rp = 29.4);
  paramvalue[11] = &(cp = 0.102e-12);
  paramvalue[12] = &(sc = 1e21);
  paramvalue[13] = &(beta = 1e-3);


  // Set the number of terminals
  setNumTerms(4);

  // Set flags
  setFlags(NONLINEAR | MULTI_REF | TR_TIME_DOMAIN);

  // Set number of states
  setNumberOfStates(2);
}

void DHLD::init() throw(string&)
{
  vt = 25.6802271e-3; q = 1.6022e-19;
  Vpara = log(vt/i01)*vt;

  // create tape
  IntVector var(2,0);
  IntVector novar;
  DoubleVector nodelay;
  var[0] = 0;
  var[1] = 1;
  createTape(var, var, novar, novar, nodelay);
}
```

```
void DHLD::eval(adoublev& x, adoublev& vp, adoublev& ip)
{
  // x[0]=state variable to compute v1 & i1
  // x[1]=state variable to compute Sn==x1
  // x[2]=dx[0]/dt  time derivative of state variable x[0]
  // x[3]=dx[1]/dt  time derivative of state variable x[1]

  adouble v1, dv1_dx, i1, dv1_dt;

 //parametrisation of the input I/V equations
 condassign(v1, Vpara - x[0], x[0] + zero, Vpara + vt*log(one + (1/vt)
            *(x[0]-Vpara)));
 condassign(dv1_dx, Vpara - x[0], one, one/(one + (1/vt)*(x[0]-Vpara)));
 condassign(i1, Vpara - x[0], i01*(exp(x[0]/vt) - one), i01*exp(Vpara/vt)
            *(one + (1/vt)*(x[0] - Vpara)) - i01);
 dv1_dt = dv1_dx * x[2];

  adouble v2 = vt*log(i1/i02 +1);
  adouble vre = i1 * re;
  adouble vj = vre + v1 + v2;
  adouble ie = a*i1 + b*i1*i1;
  adouble G = d*pow((ie/(cp/q/sc) - 2e13),2);

  adouble x1, dx1_dt;

  //parametrisation of the output photon density equation
  x1 = pow((x[1] - 2), 2) - .1;
  dx1_dt = (2*pow((x[1] - 2),1))*x[3];

  ip[0] = i1 + b*i1*i1 + tns*((i1+i01)/vt)*dv1_dt +
          c0*pow((1-vj/vd), -0.5)*( dv1_dt + (i01/i02)*exp((v1-v2)/vt)
          *dv1_dt + re*((i1+i01)/vt)*dv1_dt) + G*x1;

  vp[0] = rs*ip[0] + vj;

  ip[1] = -G*x1 - beta*ie + x1/rp + cp*dx1_dt;

  vp[1] = x1;
}

void DHLD::getLocalRefIdx(UnsignedVector& local_ref_vec,
```

```
                TerminalVector& term_list)
{
  // Make sure the vectors are empty
  term_list.erase(term_list.begin(), term_list.end());
  local_ref_vec.erase(local_ref_vec.begin(), local_ref_vec.end());

  // Insert vector elements
  term_list.push_back(getTerminal(0));
  term_list.push_back(getTerminal(1)); // Local reference terminal
  local_ref_vec.push_back(1); // Local reference index

  term_list.push_back(getTerminal(2));
  term_list.push_back(getTerminal(3)); // Local reference terminal
  local_ref_vec.push_back(3); // Local reference index
}
```

A.3 HSPICE® sub-circuit implementation, DHLD.sp

```
Double-Heterojunction Laser Diode (Rodney S. Tucker Model)
*HSPICE implementation
**********************************************************

*Is 0 100 SIN (150M 5.6M 1e9)
Is 0 100 PULSE (0M 150M 0.1N 0.1N 0.1N 8N 9N)
Vs 100 1 DC 0

* Parasitics Network

c1 103 0 0.21p
l1 103 104 1.28n
r1 104 105 0.3
c2 105 0 0.35p

r2 105 106 47.07

c3 106 0 2.38p
l2 106 107 0.33n
r3 107 108 1.12

r4 108 109 1.21
c4 109 0 7.57p
r5 108 1 3.92

Rs 1 3 2
Ve 3 4 DC 0
Re 4 5 0.468

*D1 5 6 Dm1
Gd1 5 6 CURR='2.54e-25*(exp((V(5)-V(6))/25.6802271e-3)-1)'
Rd1 5 6 1e15

*D2 6 0 Dm2
Gd2 6 0 CURR='18.13e-3*(exp(V(6)/25.6802271e-3)-1)'
Rd2 6 0 1e15

Fb 3 0 POLY(1) Ve 0 0 6.92 IC=0

* Subnetwork for evaluating I2 = tns dI1/dt
```

```
H1 20 0 Ve 1
V1 20 21 DC 0
Ctn 21 0 2.25N
*

F2 3 0 V1 1 IC=0
Cs 3 0 C='10e-12*(1/(sqrt((1-(V(3)/1.65)))))'

* Subnetwork for evaluating optical gain ''G''
Hs1 30 0 POLY(1) Ve 0 0.125 6.92
Rs1 30 0 1

Es2 31 0  VOL='1.79e-29*((V(30)/6.3662e-16)-2e13)*((V(30)/6.3662e-16)-2e13)'
Rs2 31 0 1


Gig 3 7 CURR='V(31)*V(7)'
*for beta = 1e-3
Fisp 0 7 POLY(1) Ve 0 1.25E-4 6.92E-3 IC=0
*for beta = 5e-2
*Fisp 0 7 POLY(1) Ve 0 6.25E-3 0.346 IC=0

Rp 7 0 29.4
Cp 7 0 0.102P

*.MODEL Dm1 D IS=2.54E-25
*.MODEL Dm2 D IS=18.13m
.OPTION POST INGOLD=2 NUMDGT=8

*** V(1)==input voltage terminal
*** V(7)==output photon density Sn
.print V(7)

.tran 0.002n 6n UIC
.END
```

Appendix B

VCSEL Diode Source Code

Section B.1 & B.2 contains the C++ code of the representation of the model in *f*REEDA™ .

B.1 The Header file, SVCSELD.h

```
// This may look like C code, but it is really -*- C++ -*-
//
// This is a Simple Thermal VCSEL Model
//
// by Houssam Kanj

#ifndef SVCSELD_h
#define SVCSELD_h 1

#include "../network/AdolcElement.h"

class SVCSELD : public AdolcElement
{
public:

  SVCSELD(const string& iname);

  ~SVCSELD() {}

  static const char* getNetlistName()
  {
```

```
    return einfo.name;
  }

  virtual void init() throw(string&);

  virtual void getLocalRefIdx(UnsignedVector& local_ref_vec,
              TerminalVector& term_list);

private:

  virtual void eval(adoublev& x, adoublev& vp, adoublev& ip);

  // Element information
  static ItemInfo einfo;

  // Number of parameters of this element
  static const unsigned n_par;

  // Parameter variables
  double etai, beta, tn, k, g0, n0, tp, a0, a1, a2, a3, a4, rho, n, lambda0;
  double rth, tth, t0;

  // Parameter information
  static ParmInfo pinfo[];

};

#endif
```

B.2 The C++ source code file, SVCSELD.cc

```
#include "../network/ElementManager.h"
#include "SVCSELD.h"

// Static members
const unsigned SVCSELD::n_par = 18;

// Element information
ItemInfo SVCSELD::einfo = {
  "svcseld",
  "VCSEL Model",
  "Houssam Kanj",
  DEFAULT_ADDRESS"elements/SVCSELD.h.html"
};

// Parameter information
ParmInfo SVCSELD::pinfo[] = {
  {"etai", "Injection Efficiency", TR_DOUBLE, false},
  {"beta", "Spontaneous Emission Coupling Coefficient", TR_DOUBLE, false},
  {"tn", "Carrier Reconbination Lifetime (nano sec)", TR_DOUBLE, false},
  {"k", "Scalin factor accounting for the output coupling efficiency (Watts)",
   TR_DOUBLE, false},
  {"g0", "Gain Coefficient (1/sec)", TR_DOUBLE, false},
  {"n0", "Carrier Transparency number", TR_DOUBLE, false},
  {"tp", "Photon Lifetime (sec)", TR_DOUBLE, false},
  {"a0", "1st temperature coefficient of the offset current (A)",
   TR_DOUBLE, false},
  {"a1", "2nd temperature coefficient of the offset current (A/K)",
   TR_DOUBLE, false},
  {"a2", "3rd temperature coefficient of the offset current (A/K^2)",
   TR_DOUBLE, false},
  {"a3", "4nd temperature coefficient of the offset current (A/K^3)",
   TR_DOUBLE, false},
  {"a4", "5th temperature coefficient of the offset current (A/K^4)",
   TR_DOUBLE, false},
  {"rho", "Refractive index change", TR_DOUBLE, false},
  {"n", "Refractive Index", TR_DOUBLE, false},
  {"lambda0", "Wavelength(meters)", TR_DOUBLE, false},
  {"rth", "Thermal Impedence (C/mW)", TR_DOUBLE, false},
  {"tth", "Thermal time constant (sec)", TR_DOUBLE, false},
  {"t0", "Ambient Temperature (C)", TR_DOUBLE, false}
```

```
};


SVCSELD::SVCSELD(const string& iname)
              : AdolcElement(&einfo, pinfo, n_par, iname)
{
  // Set default parameter values
  paramvalue[0] = &(etai = 1);
  paramvalue[1] = &(beta = 1e-6);
  paramvalue[2] = &(tn = 5e-9);
  paramvalue[3] = &(k = 2.6e-8);
  paramvalue[4] = &(g0 = 1.6e4);
  paramvalue[5] = &(n0 = 1.94e7);
  paramvalue[6] = &(tp = 2.28e-12);
  paramvalue[7] = &(a0 = 1.246e-3);
  paramvalue[8] = &(a1 = -2.545e-5);
  paramvalue[9] = &(a2 = 2.908e-7);
  paramvalue[10] = &(a3 = -2.531e-10);
  paramvalue[11] = &(a4 = 1.022e-12);
  paramvalue[12] = &(rho = 2.4e-9);
  paramvalue[13] = &(n = 3.5);
  paramvalue[14] = &(lambda0 = 863e-9);
  paramvalue[15] = &(rth = 2.6e3);
  paramvalue[16] = &(tth = 1e-6);
  paramvalue[17] = &(t0 = 20);

  // Set the number of terminals
  setNumTerms(12);

  // Set flags
  setFlags(NONLINEAR | MULTI_REF | TR_TIME_DOMAIN);

  // Set number of states
  setNumberOfStates(6);
}

void SVCSELD::init() throw(string&)
{
  // create tape
  IntVector var(6,0);
  IntVector novar;
  DoubleVector nodelay;
```

```
  var[0] = 0;
  var[1] = 1;
  var[2] = 2;
  var[3] = 3;
  var[4] = 4;
  var[5] = 5;
  createTape(var, var, novar, novar, nodelay);
}

void SVCSELD::getLocalRefIdx(UnsignedVector& local_ref_vec,
                TerminalVector& term_list)
{
  // Make sure the vectors are empty
  term_list.erase(term_list.begin(), term_list.end());
  local_ref_vec.erase(local_ref_vec.begin(), local_ref_vec.end());

  // Insert vector elements
  term_list.push_back(getTerminal(0));
  term_list.push_back(getTerminal(1)); // Local reference terminal
  local_ref_vec.push_back(1); // Local reference index

  term_list.push_back(getTerminal(2));
  term_list.push_back(getTerminal(3)); // Local reference terminal
  local_ref_vec.push_back(3); // Local reference index

  term_list.push_back(getTerminal(4));
  term_list.push_back(getTerminal(5)); // Local reference terminal
  local_ref_vec.push_back(5); // Local reference index

  term_list.push_back(getTerminal(6));
  term_list.push_back(getTerminal(7)); // Local reference terminal
  local_ref_vec.push_back(7); // Local reference index

  term_list.push_back(getTerminal(8));
  term_list.push_back(getTerminal(9)); // Local reference terminal
  local_ref_vec.push_back(9); // Local reference index

  term_list.push_back(getTerminal(10));
  term_list.push_back(getTerminal(11)); // Local reference terminal
  local_ref_vec.push_back(11); // Local reference index

}
```

```
void SVCSELD::eval(adoublev& x, adoublev& vp, adoublev& ip)
{
  // x[0]: terminal current, I
  // x[1]: carrier density, vn
  // x[2]: temperature, td
  // x[3]: photon density, vm
  // x[4]: output power, p0
  // x[5]: lambda, wavelenth
  // x[6]: dI/dt
  // x[7]: dvn/dt
  // x[8]: dtd/dt
  // x[9]: dvm/dt
  // x[10]: dp0/dt
  // x[11]: dlambda/dt


  adouble delta = 1e-10;
  adouble zn = 1e7;
  adouble q = 1.6e-19;
  adouble epsilon = 3.4e-23;


  vp[0] = 1.721 + 275*x[0] - 2.439e4*x[0]*x[0] + 1.338e6*x[0]*x[0]*x[0]
          - 4.154e7*pow(x[0], 4) + 6.683e8*pow(x[0], 5) - 4.296e9*pow(x[0], 6);

  ip[0] = x[0];


   adouble Ioff = a0+a1*x[2]+a2*x[2]*x[2]+a3*x[2]*x[2]*x[2]
                  +a4*x[2]*x[2]*x[2]*x[2];

   adouble N = zn*x[1] + n0;
   adouble dN_dt = zn*x[7] + 0;

   adouble S = (x[3]+0.001)/k;
   adouble dS_dt = (1/k)*x[9];

   ip[1] = (ip[0]-Ioff - q*g0*(N-n0)*S/(1+epsilon*S) -q*N/tn -q*dN_dt);
   vp[1] = N/zn;

   adouble cth = tth/rth;
```

```
    adouble Ith = (t0 + (ip[0]*vp[0] - (x[3]+delta)*(x[3]+delta))*rth);
    ip[2] = (Ith -x[2] -tth*x[8])/rth;
    vp[2] = x[2];

    vp[3] = x[3];
    ip[3] = tp*k*(-S/tp + beta*N/tn + g0*(N-n0)*S/(1+epsilon*S)- dS_dt );

    ip[4] = x[4];
    vp[4] = (k+0.25e-8)*S;

    ip[5] = x[5];
    vp[5] = lambda0*(1 - (rho/n)*(N-n0));

}
```

Appendix C

fREEDA™ Circuit Netlists

C.1 Double-Heterojunction Laser Diode

C.1.1 Time-marching Transient Analysis "tran2" with an input current pulse

The following netlist was used to generate results shown in Fig. 3.6 and Fig. 3.7.

```
Double-Heterojunction Laser Diode (Rodney S. Tucker Model)
* Time-marching Transient analysis "tran2" with a current pulse input
**********************************************************************

.tran2 tstop=6n tstep=.02n im=1 out_steps=1

vpulse:vs 1 0 v1=0m v2=150m  td=.1n  tr=.1n  tf=.1n  pw=8n  per=10n

*circuit to convert current to voltage since
*fREEDA does not have a current pulse
vsource:vp 1 11 vac=0
g:vccs1 11 2 0 0 g=-1 ri=1e16 ro=1e16

vsource:dhld_curr 2 3 vac=0v
r:rin 3 0 r=1e6

dhld:ld1  3 0 4 "oref" c0=10p beta=5e-2
```

```
open:o1 4 "oref"
res:rout 4 "oref" r=1e6
.ref "oref"

.out plot element "vsource:dhld_curr" 0 it in "curr_pulse_input"
.out plot term 3 vt in "DHLD_v_beta_5e_2_pulse_freeda"
.out plot term 4 vt in "DHLD_sn_beta_5e_2_pulse_freeda"

.end
```

C.1.2 Time-marching Transient Analysis "tran2" with a sin input current with package and chip parasitics

The following netlist was used to generate results shown in Fig. 3.9 and Fig. 3.10.

```
Double-Heterojunction Laser Diode (Rodney S. Tucker Model)
* Time-marching Transient analysis "tran2" with a sin input current
* and package and chip parasitics
**********************************************************************

.options f0=1.0e9

.tran2 tstop=10n tstep=.02n im=1 out_steps=1

isource:is0 2 0 idc=150m iac=5.6m f=f0 phase=-90

vsource:vcurrs 2 103 vac=0v

c:c1 103 0 c=0.21p
l:l1 103 104 l=1.28n
r:r1 104 105 r=0.3
c:c2 105 0 c=0.35p

r:r2 105 106 r=47.07

c:c3 106 0 c=2.38p
l:l2 106 107 l=0.33n
r:r3 107 108 r=1.12

r:r4 108 109 r=1.21
```

```
c:c4 109 0 c=7.57p
r:r5 108 3 r=3.92

dhld:ld1  3 0 4 "oref" c0=10p beta=1e-3

open:o1 4 "oref"
.ref "oref"

.out plot term 3 vt in "v_beta_1e_3_sin_tran2_freeda"
.out plot term 4 vt in "sn_beta_1e_3_sin_tran2_freeda"

.end
```

C.1.3 Harmonic-Balance Analysis "svhb" with a sin input current with package and chip parasitics

The following netlist was used to generate results shown in Fig. 3.9, Fig. 3.10, Fig. 3.11, and Fig. 3.12.

```
Double-Heterojunction Laser Diode (Rodney S. Tucker Model)
* Harmonic Balance analysis "svhb" with a single tone input
* a sin input current with package and chip parasitics
*****************************************************

.options f0=1.0e9

.svhb n_freqs=35 fundamental=f0 deriv=0 steps=0

isource:is0 2 0 idc=150m iac=5.6m f=f0 phase=-90

vsource:vcurrs 2 103 vac=0v

c:c1 103 0 c=0.21p
l:l1 103 104 l=1.28n
r:r1 104 105 r=0.3
c:c2 105 0 c=0.35p

r:r2 105 106 r=47.07
```

```
c:c3 106 0 c=2.38p
l:l2 106 107 l=0.33n
r:r3 107 108 r=1.12

r:r4 108 109 r=1.21
c:c4 109 0 c=7.57p
r:r5 108 3 r=3.92

dhld:ld1  3 0 4 "oref" c0=10p beta=1e-3

* use a big dummy resistor at the output
* port instead of an "open" element just for
* harmonic balance simulations
*open:o1 4 "oref"
res:rout 4 "oref" r=1e7

.ref "oref"

.out plot term 3 vf mag in  "v_beta_1e_3_hb_mag"
.out plot term 4 vf mag in  "sn_beta_1e_3_hb_mag"
.out plot term 3 vf invfft 10 repeat in  "v_beta_1e_3_hb_freeda"
.out plot term 4 vf invfft 10 repeat in  "sn_beta_1e_3_hb_freeda"

.end
```

C.1.4 Harmonic-Balance Analysis "svhb" with a two-tone input current with package and chip parasitics

The following netlist was used to generate results shown in Fig. 3.13.

```
Double-Heterojunction Laser Diode (Rodney S. Tucker Model)
* Harmonic Balance analysis "svhb" with a two-tone input
* current with package and chip parasitics
************************************************************
.options f0=1.0e9 f1=1.04e9
.svhb n_freqs=6 n_freqs2=6 fundamental=f0 fundamental2=f1 deriv=0 steps=0

isource:is0 2 0 idc=110m iac=5.6m f=f0 phase=-90
```

```
isource:is1 2 0 idc=110m iac=5.6m f=f1 phase=-90

vsource:vcurrs 2 103 vac=0v

c:c1 103 0 c=0.21p
l:l1 103 104 l=1.28n
r:r1 104 105 r=0.3
c:c2 105 0 c=0.35p

r:r2 105 106 r=47.07

c:c3 106 0 c=2.38p
l:l2 106 107 l=0.33n
r:r3 107 108 r=1.12

r:r4 108 109 r=1.21
c:c4 109 0 c=7.57p
r:r5 108 3 r=3.92

dhld:ld1  3 0 4 "oref" c0=10p beta=1e-3

* use a big dummy resistor at the output
* port instead of an "open" element just for
* harmonic balance simulations
*open:o1 4 "oref"
res:rout 4 "oref" r=1e7

.ref "oref"

.out plot term 3 vf mag in  "v_beta_1e_3_twotone_hb_mag"
.out plot term 4 vf mag in  "sn_beta_1e_3_twotone_hb_mag"

.end
```

C.2 VCSEL Diode

C.2.1 DC-sweep Analysis "dc" with an input current sweep

The following netlist was used to generate results shown in Fig. 4.2, 4.3, 4.4, 4.5, and 4.6.

```
Simple Thermal VCSEL Diode (Mena et al. Model)
* DC sweep analysis "dc" with an input current sweep
*****************************************************

.dc sweep="vsource:vs" start=2.6m stop=22.8m step=.01m

vsource:vs 1 0 vdc=0m

*subcircuit to convert current to voltage since current
*fREEDA implementation have only a voltage sweep
vsource:vp 1 11 vac=0
g:g1 11 2 0 0 g=-1 ri=1e12 ro=1e12

vsource:vcurrf 2 3 vac=0v

svcseld:ld1 3 0 4 "nref" 5 "tref" 6 "oref" 7 "pref" 8 "lref"

open:o1 4 "nref"

open:o2 5 "tref"

open:o3 6 "oref"

open:o4 7 "pref"

open:o5 8 "lref"

.ref "nref"
.ref "tref"
.ref "oref"
.ref "pref"
.ref "lref"

.out plot term 3 vt in "SVCSELD_v_T0_20_dc_freeda"
```

```
.out plot term 4 vt in "SVCSELD_n_T0_20_dc_freeda"
.out plot term 5 vt in "SVCSELD_t_T0_20_dc_freeda"
.out plot term 6 vt in "SVCSELD_o_T0_20_dc_freeda"
.out plot term 7 vt in "SVCSELD_p_T0_20_dc_freeda"
.out plot term 8 vt in "SVCSELD_l_T0_20_dc_freeda"
.end
```

C.2.2 Time-marching Transient Analysis "tran2" with an input current pulse

The following netlist was used to generate results shown in Fig. 4.7, 4.8, 4.9, and 4.10.

```
Simple Thermal VCSEL Diode (Mena et al. Model)
* Time-marching Transient analysis "tran2" with a current pulse input
**********************************************************************

.tran2 tstop=5n tstep=.002n im=0 out_steps=100

vpulse:vs  1 0 v1=1m v2=15m  td=0n  tr=.1n  tf=.1n  pw=4n  per=5n

*circuit to convert current to voltage since
*fREEDA does not have a current pulse
vsource:vp 1 11 vac=0
g:g1 11 2 0 0 g=-1 ri=1e12 ro=1e12

vsource:vcurrf 2 3 vac=0v

svcseld:ld1 3 0 4 "nref" 5 "tref" 6 "oref" 7 "pref" 8 "lref"

open:o1 4 "nref"
open:o2 5 "tref"
open:o3 6 "oref"
open:o4 7 "pref"
open:o5 8 "lref"

.ref "nref"
.ref "tref"
```

```
.ref "oref"
.ref "pref"
.ref "lref"

.out plot term 3 vt in "SVCSELD_v_T0_20_pulse_freeda"
.out plot term 4 vt in "SVCSELD_n_T0_20_pulse_freeda"
.out plot term 5 vt in "SVCSELD_t_T0_20_pulse_freeda"
.out plot term 6 vt in "SVCSELD_o_T0_20_pulse_freeda"
.out plot term 7 vt in "SVCSELD_p_T0_20_pulse_freeda"
.out plot term 8 vt in "SVCSELD_l_T0_20_pulse_freeda"
.end
```

C.2.3 Harmonic-Balance Analysis "svhb" with a two-tone input current with package and chip parasitics

The following netlist was used to generate results shown in Fig. 4.12, 4.15, 4.16, and 4.17.

```
Simple Thermal VCSEL Diode (Mena et al. Model)
* Harmonic-Balance Analysis ‘‘svhb’’ with a two-tone input current
* with package and chip parasitics
**********************************************************************

.options f0=1e9 f1=1.01e9

.svhb n_freqs=6 n_freqs2=5 fundamental=f0 fundamental2=f1 deriv=0 steps=0
*.svhb n_freqs=45 fundamental=f0 deriv=0 steps=0

isource:is0 2 0 idc=18m iac=0.633m f=f0 phase=-90
isource:is1 2 0 idc=0m iac=0.633m f=f1 phase=-90


vsource:vcurrs 2 103 vac=0v
r:rindummy 3 0 r=1e5

l:lp 103 104 l=2.28n
c:cp 104 0 c=0.39p
r:rs 104 3 r=76
```

```
svcseld:ld1 3 0 4 "nref" 5 "tref" 6 "oref" 7 "pref" 8 "lref" t0=100

*open:o1 4 "nref"
res:rndummy 4 "nref" r=1e5

*open:o2 5 "tref"
res:rtdummy 5 "tref" r=1e5

*open:o3 6 "oref"
res:rodummy 6 "oref" r=1e5

*open:o4 7 "pref"
res:rpdummy 7 "pref" r=1

*open:o5 8 "lref"
res:rldummy 8 "lref" r=1

.ref "nref"
.ref "tref"
.ref "oref"
.ref "pref"
.ref "lref"

.out plot term 3 vf mag in  "v_svcseld_hb_mag"
.out plot term 7 vf mag in  "sn_svcseld_hb_mag"
.out plot term 3 vf invfft 10 repeat in  "v_svcseld_hb_freeda"
.out plot term 7 vf invfft 10 repeat in  "sn_svcseld_hb_freeda"

.end
```